Zeitschrift für Physikalische Chemie Neue Folge, Bd. 136, S. 1–63 (1983)

A Network Thermodynamic Investigation of Stationary and Non-Stationary Proton Transport Through Proteins

By

Axel Brünger, Zan Schulten and Klaus Schulten

Max-Planck-Institut für biophysikalische Chemie, D-3400 Göttingen;
and Department of Physics, Technical University of Munich, D-8046 Garching,
Federal Republic of Germany

(Received March 16, 1983; in final form July 12, 1983)

Biological proton conduction / Voltage-current characteristic / Time-dependent currents / Irreversible thermodynamics

A model for the biological transport of protons in linear hydrogen-bonded chains formed from the amino acid side groups of membrane proteins has been investigated in detail. The description assumes first-order kinetics for transitions between all possible proton distributions in the hydrogen-bridged chain. The corresponding master equation is solved numerically and in some representative cases also analytically. The following time-dependent observables have been evaluated: 1) proton current at the conductor ends, 2) charge displacement within the conductor, 3) free energy decrement, and 4) state of protonation of the conductor groups. It is shown which observable conduction properties reveal features of the internal dynamics and structure of proton conductors. In particular, the following observations are considered: titration of the stationary, applied voltage-induced proton currents; coupling of the proton transport to alternating electric fields or to electric field jumps; measurement of the relaxation of the above four observables following injection or ejection of a proton. We also demonstrate the possibility of constructing heterogeneous conductors with a diodic voltage-current characteristic. Allowing the interaction between the proton conductors and injecting or ejecting group to be time-dependent, we investigated the refractory phase that exists after an initial proton current pulse and demonstrated the buffering capacity of the conductors, a function that we associate with the "blue light effect" of bacteriorhodopsin. Among the theoretical developments are an algorithm to obtain the graph of the main kinetic pathways from the solution of a high-dimensional master equation, an expression for the proton resistance of a conductor derived in the framework of linear irreversible thermodynamics, a reduction of the kinetic pathways by condensing fast processes to yield analytical expressions for the observables, and finally the analytical evaluation of relaxation times by the theory of first-passage times.

Es wird ein Modell der biologischen Protonenleitung durch Membranproteine vermittels linearer Wasserstoffbrückenketten zwischen Aminosäureseitengruppen untersucht. Die theore-

tische Beschreibung beruht auf einer Kinetik erster Ordnung für die Übergänge zwischen allen möglichen Protonenverteilungen in der Wasserstoffbrückenkette. Die entsprechende Mastergleichung wird numerisch und in einigen repräsentativen Fällen analytisch gelöst. Die folgenden vier zeitabhängigen Observablen werden berechnet: 1) Protonenstrom an den Leiterenden, 2) Ladungsverschiebung im Leiter, 3) Abnahme der freien Energie und 4) Protonierungsgrad der beteiligten Leitergruppen. Es wird gezeigt, welche beobachtbaren Leitungseigenschaften Aufschluß über die Merkmale der internen Dynamik und Struktur eines Leiters liefern. Dazu werden insbesondere betrachtet: Die Titration des stationären, spannungsinduzierten Protonenstroms, die Kopplung des Protonentransportes an elektrische Wechselfelder und Feldsprünge und die Relaxation der oben erwähnten vier Observablen nach Protoneninjektion und Protonenejektion. Ferner wird die theoretische Möglichkeit eines Protonenleiters mit diodischer Strom- Spannungs-Charakteristik nachgewiesen. Für eine Situation mit zeitabhängiger Wechselwirkung einer Leiterendgruppe mit basischen und sauren Ejektor- bzw. Injektorgruppen wird die Existenz einer refraktionären Phase eines Leiters nach einem Protonenstrompuls nachgewiesen und wird gezeigt, daß Protonenleiter eine gewisse Pufferkapazität besitzen. Die letztere Eigenschaft kann eventuell bei dem sog. ‚Blaulichteffekt' des Bakteriorhodopsin eine wesentliche Rolle spielen. Die Durchführung der Arbeit beruht auf verschiedenen methodischen Entwicklungen. Es wurde ein numerischer Algorithmus bereitgestellt, welcher von der Lösung höher-dimensionaler Mastergleichungen die zyklischen Graphen der wichtigsten kinetischen Ströme konstruiert und damit die Mechanismen der Protonenleitung nachzuweisen gestattet. Im Rahmen der linearen Näherung der Nichtgleichgewichtsthermodynamik wird ein einfacher analytischer Ausdruck für Protonenwiderstände abgeleitet. Ferner wird eine Methode zur Reduktion einer Master-Gleichung, welche schnelle Reaktionsschritte kondensiert, angegeben und damit analytische Ausdrücke für die quasistationären Werte der Observablen gewonnen. Schließlich wird mit Hilfe der ‚First Passage Time'-Verteilung eine analytische Berechnung der Relaxationszeiten von Protonenleitern ermöglicht.

1. Introduction

During the past two decades Mitchell's hypothesis postulating proton-mediated membrane potentials as the basis of the primary energy storage and transduction in respiratory and photosynthetic systems has found wide confirmation [1]. The challenge remains, however, to elucidate the molecular mechanism of the proton transport involved. A first success in this direction has been the isolation and characterization as a passive proton conductor of the F_0 fraction of the ATP-ase of thermophilic bacteria [2]. One of the most intensively studied proton transport systems is the membrane protein bacteriorhodopsin which functions as a light-driven proton pump in Halobacterium halobium (H.h.). Although proton uptake and release, internal protonation-deprotonation processes and charge displacements all have been observed for bacteriorhodopsin [3], the molecular mechanism of the proton transport through the protein is still unknown. Direct observation of these conduction pathways is difficult since the transport involves only minor motions of the protein backbone or side groups. Furthermore, since only a small number of protons suffice for proton translocation, the

elementary processes involved may go unnoticed in many observations. These difficulties necessitate that the experimental investigations be supported by theoretical investigations which test the realization of molecular models and derive suitable observables to identify transport mechanisms.

Passive proton transport across membrane proteins (i.e. transport down the electrochemical potential existing across the membrane) is likely to be simpler than active transport, and an understanding of the former should contribute to progress in elucidating the latter. Current ideas concerning passive proton transport center around an involvement of the acidic and basic amino acid side groups. Such a role is supported by the known structural details of bacteriorhodopsin [4]. The mechanism is based on the works of Eigen [5] and Onsager [6] which were initially concerned with proton conduction in water and ice. Already in 1967 Onsager suggested how these mechanisms could be used to transport protons along a hydrogen-bridge network created from the amino acid side groups of membrane proteins. Recently Nagle and Morowitz [7] and Dunker [8] have advanced this suggestion as the fundamental pathway for proton conduction in ATPase and H.h. For non-biological systems, e.g. ice and imidazol, there exist detailed quantum mechanical investigations of proton transport [9, 10]. For biological systems most studies have been mainly qualitative and have refrained from quantitative statistical mechanical calculations. Two notable exceptions are the theoretical works of Läuger [11] and Nagle, *et al.* [7]. Läuger treated ion transport through biological "pores" using a kinetic model in which the ion jumps over barriers and in which the pore contains at most one ion. Nagle, *et al.* [7], using the simplest conduction mechanism consistent with the Onsager model, considered several important proton transport situations arising in bioenergetics and obtained estimates for the membrane crossing times for a proton in a homogeneous, i.e. identical groups, hydrogen-bridge network. We have recently started a detailed theoretical investigation on the basis of the Onsager model and evaluated proton currents on the basis of the molecular properties of participating side groups [12].

Previous theoretical investigations of proton conduction, particularly on non-biological systems, concentrated mainly on the fast processes, motion of a proton in a hydrogen-bridge potential and collective oscillations of protons in a hydrogen-bridge network. An extension of these studies to also include the slower elementary processes in an overall description of proton conduction appears to be feasible only at the price of an approximation which assumes Poisson statistics, i.e. first-order kinetics, for all elementary processes. This approximation results in a master equation for the allowed transitions between all proton distributions occurring in the conductor. In [12] this master equation has been solved to yield the stationary transport rate for conductors composed of homogeneous, i.e. identical groups. In the following these investigations will be extended to include heterogeneous

conductors, non-stationary situations as well as time-varying external potentials. In particular, the relaxation of conductors after ejection or injection of a proton, a process of interest in connection with bacteriorhodopsin, is considered. The main aim is to evaluate relevant quantities, i.e. proton currents, free energy decrements, charge displacements, and protonation states, which are amenable to experimental observation.

We describe the proton conduction in a hydrogen-bridge network in terms of intermediate, thermally activated faults which are schematically presented in Fig. 1. The protein spans the membrane and the side groups labeled X form a one-dimensional conductor that transports protons from side a to side b. In thermal equilibrium with the solutions at both sides at neutral pH, a homogeneous conductor contains one proton for each group oriented such that adjacent groups are hydrogen bonded through one proton. The faults in Fig. 1 represent deviating situations in that either no proton is situated on a group (L_t fault) or two protons are situated on a group (D_t fault) or no proton is located between two adjacent groups (L_r fault) or two protons are located between adjacent groups (D_r fault). The fault-mediated conduction mechanism is reminiscent of electronic semi-conductors. By analogy to electronic components one may envisage constructing a proton diode from suitable side groups, a device particularly well adapted to the mainly unidirectional flow of protons over energy tranducing membranes. We will demonstrate that proton diodes can be realized either by a combination of acidic and basic side groups or, following a suggestion of Edmonds [13] on aqueous pores for ion conduction, by the presence of internal electric fields generated from properly oriented dipoles of the backbone and side groups of the protein.

It is not difficult today to measure a net transmembrane proton current between two reservoirs. However, to detect the few protons actually moving at an instance through a conductor is a difficult problem. These protons are only a minor fraction of the charges connected with a membrane and its constituent proteins. As a contribution to the development of methods to observe protons in a conductor, we consider here two equivalent possibilities based on coupling the proton conduction to external electrical fields, either oscillating or a jump with a rectangular pulse. Obviously all charges in a membrane probe will respond to such fields. However, we will show that the conducted protons exhibit characteristic dielectric responses in the range 10^3 Hz to 10^{10} Hz which may be detectable in certain frequency windows left open by a corresponding inertia of the remaining charges.

The sectioning of this publication will precede in the following manner. In Section 2 we set up the master equation for the description of the proton transport and introduce the necessary (pseudo) first-order rate constants for the transitions between proton configurations. In Section 3 we study the stationary transport through homogeneous and heterogeneous conductors. Considerable effort has been given to develop an algorithm to find and display the proton configurations constituting the conduction

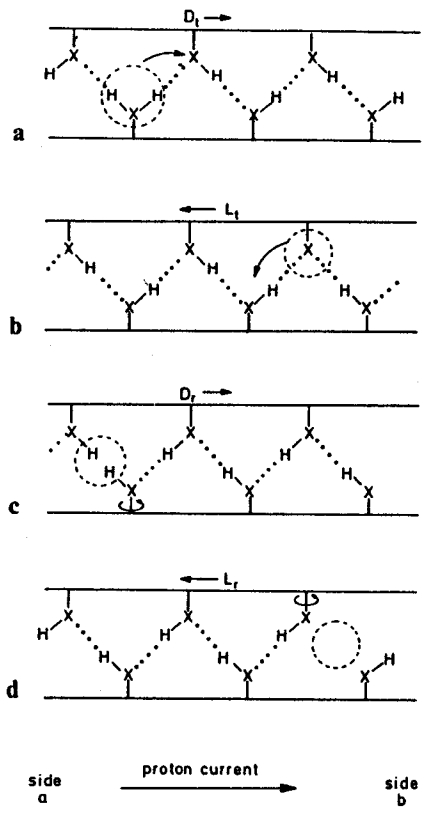

Fig. 1. Amino acid side groups X of a protein spanning a biomembrane are suggested to conduct protons by forming linear hydrogen-bridge chains. The peptide bond backbones of two adjacent α-helices are represented by pairs of straight lines. The groups X can differ from each other (heterogeneous conductor) and may include molecules of bonded water. At equilibrium the hydrogen-bridge chain entails a proton distribution with *one* proton between two neighbouring groups, the proton being in closer proximity to one of the two groups as in a typical hydrogen bridge; also each group X has only *one* proton in close proximity. The proton transport involves the generation and migration of four types of defects, the defects representing deviations from the equilibrium structure. The four defects are illustrated above: (a) the D_t fault representing a situation with *two* protons proximate to one group, (b) the L_t fault representing a situation with *no* proton proximate to a group, (c) the D_r fault representing a situation with *two* protons between two neighbouring groups, (d) the L_r fault representing a situation with *no* proton between two neighbouring groups. The D_t and L_t faults are generated by protonation and deprotonation of the conductor ends, the fault migration involves proton *translation* between neighbouring groups, i.e. the jump from a site more proximate to one group to the site more proximate to the other group; the sites are the two minima of the double well potential describing the corresponding hydrogen bridge. The D_r and L_r faults are generated and migrate by *rotation* of the side groups which thereby transport protons from one side to the other side of the groups. Structural details of hydrogen-bridge chains are discussed in [7, 8]

pathways. These cycles are determined from the master equation using network theory and some helpful results of Schnakenberg [14]. For systems near equilibrium, we derive a linear relationship between the currents through linear or non-linear (branched) pathways and the general thermodynamic force or proton affinity. In Sections 4 and 5 we investigate nonstationary transport after proton injection and ejection, the refractory phase of a conductor after a proton pulse, and the "blue light effect" of bacteriorhodopsin, i.e. an alternation of proton injection and ejection at one conductor end. We characterize the relaxation of the proton conductors and diodes by the evaluation of several time-dependent observables: 1) the changes in the conductor's dipole moment, 2) the free energy change, and 3) the integrated proton currents. The time constants for every step in the relaxation process are evaluated from the mean first-passage time approximation. In Section 6 we describe the response of the proton conductors to oscillating and pulsed electrical fields.

2. Theoretical description of the model

The model we adopt for the proton conductor is a linear chain of $N-1$ hydrogen bridges formed by N side groups of a protein (see Fig. 1). In thermal equilibrium at neutral pH, a chain of homogeneous side groups contains approximately one proton in each bridge. Also during conduction, a condition necessitating a deviation from thermal equilibrium, one expects about N protons in such a conductor. Because of the strong interaction between protons in the chain, the basic entity for theoretical description of proton transport is not a single proton, but rather all possible distributions of $N, N \pm 1, N \pm 2, \ldots$ protons. We call these particular distributions "proton configurations". Elementary processes in the conductor are transitions between two proton configurations. We assume that the elementary processes are independent and obey first-order kinetics.

If one numbers the proton configurations in a suitable way and represents the state of the conductor by a vector $P(t)$, the i-th component giving the probability of the i-th configuration to be realized, then the dynamics of the proton motion is described by the master equation

$$\frac{\mathrm{d}}{\mathrm{d}t} P = \dot{P} = \mathbf{K}\, P. \tag{2.1}$$

The off-diagonal elements of the rate matrix K_{ij} are the first-order rate constants for the elementary process producing the transition from the $j \to i$ configuration. Except for the (de-) protonation processes (cf. 2.6), the rate constants for motions of the protons within the conductor are given by

$$K_{ij} = A_{ij} \exp\left(-\beta E_A^T\right) \tag{2.2}$$

where $\beta = 1/kT(\mathrm{K}^\circ)$. In this Arrhenius form, A_{ij} is the frequency factor and E_A^T the total activation barrier for the transition $j \to i$

$$E_A^T = E_A \pm \mu\,(\Delta V_{\mathrm{ext}} f - \Delta V_{\mathrm{int}})/2d. \tag{2.3}$$

E_A^T includes contributions of external and internal electric fields. The internal field can arise, for example, from dipoles aligned along the protein backbone. μ is the change in the dipole moment accompanying the respective motion of the protons. f is the fraction of the applied external field acting on the internal groups. d is the width of the membrane. The sign in (2.3) is chosen negative if the motion is in the direction of the defined orientation from the left to the right end of the conductor (from side a to side b in Fig. 1). The fields ΔV_{ext} and ΔV_{int} are similarly oriented. All calculations are performed with $T = 298\,^\circ\mathrm{K}$. The conservation of total probability require the diagonal elements of K to be

$$K_{ii} = -\sum_{j \neq i} K_{ji}. \tag{2.2b}$$

We assume, as shown in Fig. 1, that each amino acid side group can accept at most two protons. The states XH_2 with two protons and X without protons are called ionic defects, and since these defects move by translation of a proton between two groups, they are labeled D_t and L_t faults, respectively. In the hydrogen bridges between the conductor groups, so-called Bjerrum type faults can be generated either due to the absence of protons in the bridge [Bjerrum (L) fault] or due to the presence of two protons in the bridge [Bjerrum (D) fault]. These faults move by rotation of the groups about the protein-group bond, and hence are labeled D_r and L_r.

In our calculations we have restricted the elementary processes within the conductor to rotations of single groups or to translations of single protons between two adjacent groups, and we have neglected interactions between faults. For example, we have not included processes which involve the concerted translation of protons in adjacent hydrogen bridges [15], a process of considerable interest since it circumvents the formation of ionic faults in the conductor. Neither did we include the interesting cooperative effect predicted for hydrogen-bridge chains [16] whereby the energy of formation of a hydrogen bridge is a function of the length N of the chain, an effect which leaves the formation energies of faults nonadditive. These restrictions are not a prerequisite of the theory presented here, but rather have been adopted to simplify a first approach to the problem of proton transport.

The values assumed in our calculations for the activation energies E_A of rotational and translational fault migration as well as the corresponding changes of the dipole moment μ_r and μ_t of the conductor are provided in Table 1. The transport of a proton charge e across the whole membrane of width d requires $N-1$ translations and N rotations and leads to an overall change in the dipole moment $ed = (N-1)\,\mu_t + N\mu_r$ of the system. The rate

Table 1. *Internal proton motions*

Process		Activation energy/eV	Activation energy/eV of inverse process	Change of dipole moment
Migration of ionic (D) defect[a]	$D_t^Y \rightarrow D_t^X$	0.02	$0.02 + 2.3\,[pK(XH_2^+) - pK(YH_2^+)]/\beta$	$\mu_t \equiv \dfrac{ed}{1.56N-1}$
Migration of ionic (L) defect[b]	$L_t^Y \rightarrow L_t^X$	0.04	$0.04 + 2.3\,[pK(YH) - pK(XH)]/\beta$	
Destruction of (LD) defect[c]	$L_t^X D_t^Y \rightarrow O$	E_{LD}[d]	$E_{LD} + 2.3\,[pK(XH) - pK(YH_2^+)]/\beta$	
Migration of Bjerrum (L) fault	$L_r^X \rightarrow L_r^Y$	0.24	0.24	$\mu_r = 0.56\,\mu_t$
Migration of Bjerrum (D) fault	$D_r^X \rightarrow D_r^Y$	0.24	0.24	
Creation of Bjerrum (LD) fault	$O \rightarrow L_r^X D_r^Y$	0.94	0.24	
Creation of Bjerrum (L) fault[e]	$O \rightarrow L_r$	0.44	0.24	
Creation of Bjerrum (D) fault[e]	$O \rightarrow D_r$	0.74	0.24	

[a] Without restriction $pK(XH_2^+) \geq pK(YH_2^+)$
[b] Without restriction $pK(YH) \geq pK(XH)$
[c] $pK(XH) > pK(YH_2^+)$; otherwise the expressions for the forward and reverse processes as well as pK (XH) and pK (YH_2^+) are exchanged
[d] $E_{LD} = 0.04$ between homogeneous groups, $E_{LD} = 0.35$ between heterogeneous groups A and B of the proton diode in Sections 3–6
[e] Only at end groups possible

constants K_{ij} resulting from the activation energies in Table 1 with the frequency factor

$$A_{ij} = 10^{11}\mathrm{s}^{-1} \tag{2.4}$$

are based on values determined from proton transport in ice and are identical to rates employed in [12]. The necessary modifications to consider transitions between heterogeneous groups are also given in Table 1 and will be discussed in greater detail in section 3.4 where they are first employed in calculations.

We will later represent the rate constants constructed from (2.2) by K(process), e.g. $K(D_t \rightarrow D_t)$ is the rate constant for the migration of an ionic D_t fault in the a → b direction and $K(D_t \leftarrow D_t)$ accounts for migration in the opposite direction. The rate constants for the migration of ionic D_t or L_t faults are determined to be 10^4 times faster than the migration of an L_r fault. One obtains from Table 1 with (2.4), $K(D_t \rightarrow D_t) = 5 \cdot 10^{10}\mathrm{s}^{-1}$ and $K(L_r \rightarrow L_r) = 7 \cdot 10^6\mathrm{s}^{-1}$. Rotation of an end group to create an L_r fault in the conductor is considerable slower, $K(O \rightarrow L_r) = 4 \cdot 10^3\mathrm{s}^{-1}$. Unfortunately, there are few measurements of the rotations of amino acid side groups in proteins available for comparison. Using high resolution NMR spectroscopy Wüthrich, *et al.* [17] have measured the rotation of tyrosine and phenylalanine groups in globular proteins. They determined that the aromatic rings undergo 180°flips about the $C_\beta - C_\gamma$ bonds with a rate constant of $10^4 - 10^2\mathrm{s}^{-1}$ depending upon the position within the protein. Pecht, *et al.* [18] have, however, measured a rotation rate for tryptophan in the subnanosecond range. Since only the ratio between the rotation and jump rate constants is relevant for proton transport, we have extended our calculations to include the case of group rotations becoming as fast as the proton translation processes.

For processes moving protons in the direction of strong fields, E_A^T as given in (2.3) can assume negative values. There is, however, no physical basis for an application of the Boltzmann factor with negative activation energy to yield a rate constant larger than the frequency factor A_{ij}. We will, therefore, assume that A_{ij} is the upper limit for the rate constants K_{ij}. To obey detailed balance, we replace in the case $E_A^T < 0$, K_{ij} by the corrected values $\bar{K}_{ij}$,

$$\bar{K}_{ij} = A_{ij},\ \bar{K}_{ji} = A_{ij}K_{ji}/K_{ij}. \tag{2.5}$$

The rate constants for protonation and deprotonation of the conductor end groups are taken to be [29]

$$K_{ij} = K_P(\mathrm{B}) = 2 \cdot 10^{10}[10^{-\mathrm{pH}} + 10^{\mathrm{pK(BH)} + \Delta\mathrm{pK} - 14}]$$

$$K_{ji} = K_D(\mathrm{BH}) = 2 \cdot 10^{10}[10^{-\mathrm{pK(BH)} - \Delta\mathrm{pK}} + 10^{\mathrm{pH} - 14}] \tag{2.6}$$

where B is either the unprotonated (X) or singly protonated (XH) end group. ΔpK provides a correction to the pK values of the conductor end groups due

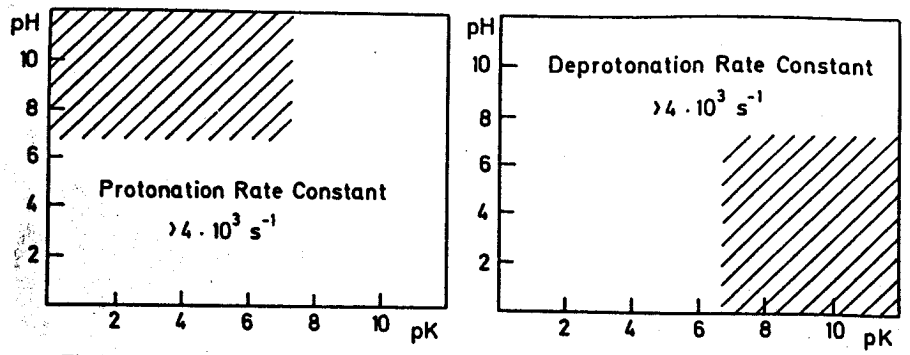

Fig. 2. Rate constants for protonation K_P and deprotonation K_D evaluated according to Eq. (2.6); the shaded areas indicate values less than $4\cdot10^3 s^{-1}$, i.e. the corresponding rate constant for a neutral group (pK = 7) at neutral pH (pH = 7)

to the membrane potential and internal electric fields. For the proton diodes in Sections 3, 4, and 6 such a field dependence is assumed, and the correction ΔpK is set to

$$\Delta\mathrm{pK} = \pm\, e\beta[\Delta V_{\mathrm{ext}}(1-f) + \Delta V_{\mathrm{int}}]/(2\cdot\ln 10), \quad f=(N-1)/(N+1). \quad (2.7)$$

The positive sign in (2.7) is selected if the proton motion is in the direction of the defined orientation $a \to b$. For homogeneous conductors, we set ΔpK = 0 and $f = 1$.

The deprotonation and protonation steps will influence the transport only in those pH-pK ranges where K_D or K_P are of the same or smaller order of magnitude as the internal motions. For a neutral group at neutral pH (pK = pH = 7), $K_D = K_P = 4\cdot10^3 s^{-1}$ which is about as fast as the formation of an L_r rotational fault. In Fig. 2 we have indicated the pH-pK ranges in which the (de-) protonation rate constants would be smaller than those of a neutral group.

With the rate constants defined above, one can show that the potential difference which induces the proton current is the electrochemical potential

$$\Psi = \Delta V_{\mathrm{ext}} + \frac{\ln 10}{\beta e}\,\Delta\mathrm{pH} \quad (2.8)$$

and is independent of the internal fields and activation energies in Table 1. The proof starts from the following observation: The affinity of a cycle connecting a set of proton configurations, e.g. $i \to j \to k \to l \to i$, is defined as [14]

$$\mathcal{A} = \ln \Pi\ K_{ji}/K_{ij}$$

where the product is taken over all $i \to j$ steps of the cycle in one direction

corresponding to $a \to b$ transport. This quantity is the same for all cycles which imply the transport of one proton. This result follows from the fact that detailed balance holds for all steps (elementary processes) except the (de-)protonation processes, for which holds

$$K_P/K_D = 10^{-\mathrm{pH}+\mathrm{pK}+\Delta\mathrm{pK}}. \quad (2.9)$$

Furthermore, one can show that the potential $\frac{1}{e\beta}\mathcal{A}$ which drives a stationary flow through a cycle is identical to Ψ in (2.8).

It is often necessary for a numerical solution of the master equation to reduce the large number of possible proton configurations. For closed systems like a proton conductor in contact with a single reservoir, i.e. systems for which detailed balance holds for all steps, one can assign a formation energy E_F to each configuration and include in a calculation only configurations below a certain energy limit $E_F^{\max}$. In the case of open systems, like a proton conductor in contact with two different proton reservoirs, formation energies cannot uniquely be assigned. In fact, the formation energies of ionic D_T and L_T faults depend on the reservoir at which they have been generated. One may, however, assign uniquely an approximate formation energy for the ionic faults at a group X_i between the end groups X_1 and X_N ($1 \le i \le N$) by means of the interpolation formula

$$E_F(\mathrm{D}_{\mathrm{T}}^{\mathrm{X}_i}) = E_F(\mathrm{D}_{\mathrm{T}}^{\mathrm{X}_1}) + \frac{(i-1)}{(N-1)}\cdot[E_F(\mathrm{D}_{\mathrm{T}}^{\mathrm{X}_N}) - E_F(\mathrm{D}_{\mathrm{T}}^{\mathrm{X}_1})]$$

$$E_F(\mathrm{L}_{\mathrm{T}}^{\mathrm{X}_i}) = E_F(\mathrm{L}_{\mathrm{T}}^{\mathrm{X}_1}) + \frac{(i-1)}{(N-1)}\cdot[E_F(\mathrm{L}_{\mathrm{T}}^{\mathrm{X}_N}) - E_F(\mathrm{L}_{\mathrm{T}}^{\mathrm{X}_1})] \quad (2.10a)$$

where

$$E_F(\mathrm{D}_{\mathrm{T}}^{\mathrm{X}_{1,N}}) = -\beta^{-1}\ln(K_P/K_D) \quad (2.10b)$$

with $\mathrm{pK} = \mathrm{pK}(\mathrm{X}_{1,N}\mathrm{H}_2^+)$ and ΔpK = 0 in (2.6) and

$$E_F(\mathrm{L}_{\mathrm{T}}^{\mathrm{X}_{1,N}}) = -\beta^{-1}\ln(K_D/K_P), \quad (2.10c)$$

with $\mathrm{pK}(\mathrm{X}_{1,N}\mathrm{H})$ and ΔpK = 0 in (2.6).

The energy of formation of the neutral Bjerrum L_r and D_r faults are uniquely set to

$$E_F(\mathrm{L}_r) = 0.2\,\mathrm{eV}$$
$$E_F(\mathrm{D}_r) = 0.5\,\mathrm{eV}. \quad (2.11)$$

The formation energy for a proton configuration is then taken to be the sum of the energies of all faults involved, evaluated according to Eqs. (2.10) and

(2.11). A selection criterium based on an energy limit can then be also applied to proton conductors between two reservoirs. The appropriate energy limit E_F^{max} has been established by convergence tests.

3. Stationary transport

3.1. Numerical Solution of the Master equation

For any pair of the 2^{2N} proton configurations of an N-group conductor, there exists a set of transitions among the elementary processes discussed in Section 2 connecting the two configurations. Or in other words, the graph corresponding to the non-zero elements of the rate matrix **K** in the master Eq. (2.1) is strongly connected. According to a generalization of Kirchhoff's theorem in [14] there exists exactly one normalized steady-state solution P° of (2.1)

$$\mathbf{K}\, P^\circ = 0. \tag{3.1}$$

It has the properties

$$0 \le P_i^\circ \le 1, \quad 1 \le i \le 2^{2N}$$

$$\sum_{i=1}^{2^{2N}} P_i^\circ = 1. \tag{3.2}$$

P° can be determined numerically by rewriting the steady-state condition (3.1)

$$\sum_{\substack{j=1 \\ j \neq k}}^{2^{2N}} (P_j^\circ / P_k^\circ)\, K_{ij} = -K_{ik},\ i = 1,2,\ldots 2^{2N},\ i \neq k. \tag{3.3}$$

For the sake of numerical stability, P_k° should be large; and therefore, the row of **K** corresponding to the configuration k with the lowest formation energy (Section 2) has been written on the r.h.s. of (3.3). It can be solved numerically as an inhomogeneous linear system with maximal rank to obtain P° up to the scale factor $1/P_k^\circ$. If one neglects certain configurations by the application of the energy criterium in Section 2, several nonconnected (disjunct) subspaces can occur. Each subspace may be treated separately; and therefore, we consider without restriction an irreducible master equation with a strongly connected graph.

Because of the conservation of total probability (2.2b), the master equation can be re-written

$$\dot{P}_i = \sum_j K_{ij} P_j = \sum_j (K_{ij} P_j - K_{ji} P_i) = \sum_j F_{i \leftarrow j}. \tag{3.4}$$

$F_{i \leftarrow j} = K_{ij} P_j - K_{ji} P_i$ is the flux connecting directly proton configuration j and i. For the steady-state solution P° Kirchhoff's current law

$$\sum_j F_{i \leftarrow j}^\circ = 0 \tag{3.5}$$

holds for every configuration i. The steady-state flux of protons across the conductor end groups can be expressed in terms of the transitions involving protonation of either the left or right end group:

$$J_L = \Sigma\, F_{i \leftarrow j}^\circ \quad (i \leftarrow j) \text{ protonation left side}$$

$$J_R = -\Sigma\, F_{i \leftarrow j}^\circ \quad (i \leftarrow j) \text{ protonation right side} \tag{3.6}$$

where the summation extends over all disjunct subspaces of (3.1). Under steady-state conditions, the flux J_L must equal J_R. This equality was checked as a non-trivial test for the numerical stability of the solutions.

In our numerical procedure we first select all proton configuration with an (approximate) energy of formation smaller than E_F^{max} and store this basis with labels indicating the position as well as the type of defects and formation energy. With an option all configurations with D_t faults, i.e. with two protons on some groups, can be excluded. The transitions allowed according to Table 1 are determined, coded, and stored. Next the disjunct subspaces of the master equation are searched for and treated separately. For each subspace the corresponding matrix of the master equation (3.1) is generated. The steady-state solution P° is determined according to (3.3) by use of a standard routine for inhomogeneous, linear systems [19]. The local fluxes $F_{i \leftarrow j}^\circ$ and the total steady-state flux $J_R(J_L)$ are calculated by means of Eqs. (3.4) and (3.6).

To identify the most important configurations involved in the proton transport, we construct a subset Φ_ε of all transition fluxes $F_{i \leftarrow j}^\circ$. The elements of Φ_ε are those fluxes satisfying

$$|F_{i \leftarrow j}^\circ| > \varepsilon \max_{i,j} |F_{i \rightarrow j}^\circ| \tag{3.7}$$

where ε is the largest value smaller than 0.1 such that the current law (3.5) is fulfilled within 10%. From the reduced graph connecting all transitions occuring in Φ_ε, the proton configurations and pathways involved in the transport can readily be seen. The graph itself which may be branched and looped in an arbitrary way is transformed into a linear structure for output on a line printer. Because of the complexity of the problem, in particular the handling of the graphs, we had to resort to use of a high order computer language like PASCAL with sophisticated data structures and recursive procedure calls.

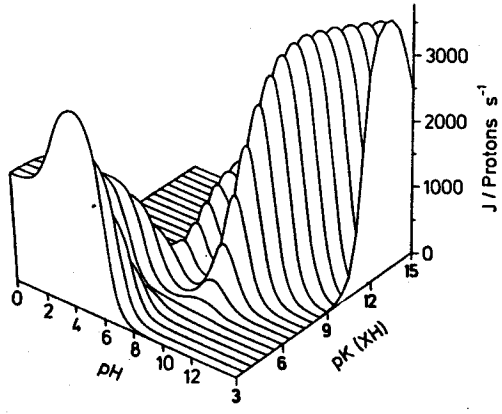

Fig. 3. Stationary proton current ($J = J_R = J_L$) across a homogeneous chain of $N = 4$ side groups capable of accepting only a single proton as a function of the group pK(XH) and $pH = pH_a = pH_b$, i.e. identical solution pH on both sides of the conductor. The current is induced by an external electrical potential, $\Delta V_{ext} = 100\,mV$

3.2. Transport in homogeneous conductors

In this section we examine the dependence of the stationary proton current through a homogeneous conductor upon the conducting group's pK, the pH, and applied external voltage. Already in [12] and by repeated tests we determined that a change in the conductor's length (number of groups N) introduced no new important phenomena, so that a short conductor can serve as a prototype for longer chains. For the sake of convenience in the analysis and computer time, we have used in the following calculations conductors with four identical side groups.

We consider first a conductor composed of side groups accepting only a single proton, e.g. tyrosine. Figure 3 shows the stationary current induced by a 100 mV potential difference as a function of the pH of the surrounding solution as well as the pK of the conducting groups. Appreciable currents are seen to arise only when the solution pH is in the neighborhood of the group's pK value. This finding suggests that one may experimentally identify the pK-range of the conducting groups by titration under fixed electrical potential conditions.

To analyze the mechanism underlying the proton current in Fig. 3 we must determine which route through the space of proton configurations produces the current. For this purpose we consult the Φ_ε-graph of the dominant transition fluxes between proton configurations. In most cases we find that only one or two cycles of proton configurations contribute. It is well known that the stationary flux through a kinetic pathway is rate limited by

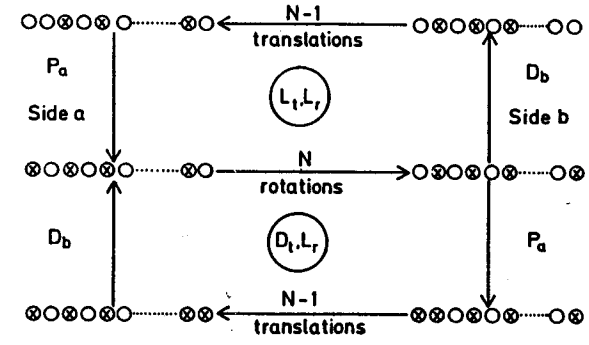

Fig. 4. The $(L_t - L_r)$ and $(D_t - L_r)$ single file cycles (see text)

the slowest transitions. Hence, one can simplify the description of the cycle fluxes by condensing the many transitions involved in the cycle to a small number of effective transitions. This reduction provides simple expressions for the proton current which in many cases are found to agree well with the predictions of the extended numerical calculations. The value of this analysis is that the key elementary processes of the proton conduction pathways are identified. Which pathways are involved depends, however, strongly on the pH and pK range and, hence, a unified analysis is not possible.

We consider first conduction at low pH values, pH < pK. The Φ_ε-graph shows that in this case the primary pathway involves a single file migration* of L_t and L_r faults. The corresponding cycle is shown in the top half of Fig. 4. The transport is initiated by removing a proton from the conductor. The resulting hole (L_t fault) then migrates across the chain to the other end where protonation takes place. The conductor returns to its original configuration by successive rotations of the side groups (L_r fault migration).

Using the values for the internal motions given in Table 1 together with (2.4), one can deduce that a jump of a proton between groups ($\simeq 10^{10}\,s^{-1}$) occurs considerably faster than the rotation of a side group ($\simeq 10^{7}\,s^{-1}$). The slowest motion within the conductor is then the rotation of the end group that creates the L_r fault [$K(L_r \leftarrow 0) = 4 \cdot 10^3 s^{-1}$]. As indicated in Fig. 2, for pH < pK protonation [K_P(X)] is always faster than the process $L_r \leftarrow 0$ whereas the classification of the deprotonation process [K_D(XH)] varies, depending on pH and pK. Consequently the flux will be approximately determined by either K_D or $K(L_r \leftarrow 0)$. Following Läuger [11] and Nagle *et al.* [7] we have constructed in Fig. 5a a qualitative free energy profile of the $(L_t - L_r)$ single file cycle for pX(XH) = 12 and pH = 6. To assign the barrier

* Linear sequencial transport in configuration space

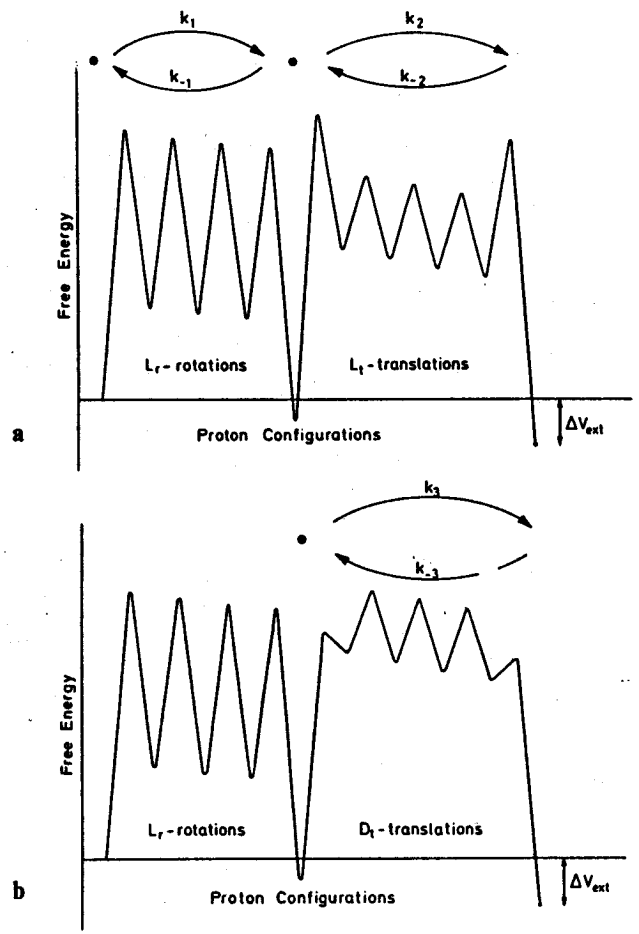

Fig. 5. Free energy profiles of the proton transport by a homogeneous conductor (pK = 12) at pH = 6: a) for the ($L_t - L_r$) cycle of Fig. 3, and b) for the ($D_t - L_r$) cycle of Fig. 7

heights from the rate constants including those for the (de-)protonation step, we have assumed that they all can be expressed by an Arrhenius form so that

$$\text{barrier height } (j \to i) = (\ln A_{\max} - \ln K_{ij})/\beta.$$

Since the (de-)protonation rate constants can become larger than the frequency factor A_{ij} (2.4) used to evaluate the rate constants for the internal motions, we have taken $A_{\max} = 10^{13} \simeq kT/h$ to avoid negative activation

barriers. High barriers indicate slow transitions and low barriers indicate fast transitions. Figure 5a also shows that upon completion of the cycle a conducted proton has experienced an energy loss equal to ΔV_{ext}.

As discussed in [12] the rotations in the single file mechanism can be treated as a gambler's ruin problem, i.e. a one-dimensional discrete random walk between two absorbing barriers. The probability that an L_r fault created at the end b migrates to the end a is

$$P_{b \to a} = (1 - s)/(1 - s^N), \tag{3.8a}$$

whereas the probability for the reverse process is

$$P_{a \to b} = (s^{-1} - 1)/(s^{-N} - 1) = s^{N-1} P_{b \to a}. \tag{3.8b}$$

Here s is a bias measure given by the ratio of the probability that the fault rotates toward b to the probability that it rotates toward a. With the defined orientation in Section 2, s is the ratio of the rate constant for L_r migration with the field $K(L_r \to L_r)$ to the value against the field $K(L_r \leftarrow L_r)$. N is the number of groups in the conductor, in our case $N = 4$. The 100 mV applied voltage that induces the current biases the migration such that

$$s = K(L_r \to L_r)/K(L_r \leftarrow L_r) = \exp(-\beta \mu_r \Delta V_{ext}). \tag{3.9}$$

One can then condense the L_r rotations in Fig. 5a into one effective transition described by the effective rate constants k_1 and k_{-1} which can be evaluated with the aid of Table 1 and (2.2) – (2.4)

$$\begin{aligned} k_1 &= K(L_r \leftarrow 0)\ P_{b \to a} = 1885 \text{ protons s}^{-1} \\ k_{-1} &= K(0 \to L_r)\ P_{a \to b} = 356.9 \text{ protons s}^{-1}. \end{aligned} \tag{3.10}$$

Since the rotational motions are taken to be independent of pH and pK (see Table 1) this reduction can always be done. The effective rate constants satisfy a consistency condition

$$k_1/k_{-1} = \frac{K(L_r \leftarrow 0)}{K(0 \to L_r)} [K(L_r \leftarrow L_r)/K(L_r \to L_r)]^{N-1}. \tag{3.11}$$

A similar reduction of the successive proton translations is possible, so that the single file cycle can be schematically represented by the two step system

$$A \underset{k_{-1}}{\overset{k_1}{\rightleftharpoons}} B \underset{k_{-2}}{\overset{k_2}{\rightleftharpoons}} A. \tag{3.12}$$

$k_{\pm 2}$ are the effective forward and backward rate constants describing the deprotonation of the conductor and subsequent translation of the hole

(L_t fault) across the conductor. Since protonation is slower than migration of the L_t fault

$$k_{+2} = K_D^b(\mathrm{XH}) \frac{P_{b\to a} K_P^a(\mathrm{X})}{P_{b\to a} K_P^a(\mathrm{X}) + P_{a\to b} K_P^b(\mathrm{X})} \tag{3.13}$$

$$k_{-2} = K_D^a(\mathrm{XH}) \frac{P_{a\to b} K_P^b(\mathrm{X})}{P_{a\to b} K_P^b(\mathrm{X}) + P_{b\to a} K_P^a(\mathrm{X})}$$

where $P_{b\to a}$ is evaluated from (3.8) with

$$s = \exp(-\beta\mu_t \Delta V_{\mathrm{ext}}/d) = K(\mathrm{L_t} \to \mathrm{L_t})/K(\mathrm{L_t} \leftarrow \mathrm{L_t}). \tag{3.14}$$

For the case that $K_P(\mathrm{X}) = K(\mathrm{L_t} \to \mathrm{L_t})$, $k_{\pm 2}$ are just the gambler's ruin expressions for $N+1$.

The proton current J can now be estimated by solving for the steady-state flux of the reduced cycle (3.12) exactly. One obtains at pK = 12 and pH = 6 the rate constants $k_2 = 180.6\,\mathrm{s}^{-1}$ and $k_{-2} = 19.43\,\mathrm{s}^{-1}$ and

$$J = \frac{k_1 k_2 - k_{-1} k_{-2}}{k_1 + k_{-1} + k_2 + k_{-2}} = 136.5 \text{ protons s}^{-1} \tag{3.15}$$

which is within one percent of the numerical value of 136.2 protons s^{-1} in Fig. 3. From the values of $k_{\pm 1}$ and $k_{\pm 2}$, it is clear that the translational sequence determines the current for basic side groups when the pH is considerably less than the group's pK. As the pH approaches the pK value, deprotonation can become so fast that the rotational sequence will limit the current. For acidic side groups with pH < pK, the rotational sequence will primarily determine the current.

The translational-rotational single file cycle just discussed is the principal conduction pathway for neutral side groups at neutral pH as well. The reduced cycle, however, must be generalized to include three steps as shown in Section 3.4. In this case both the protonation and deprotonation of the end groups are as slow as the formation of the rotational L_r fault, and the current through the single file cycle goes through a minimum.

As the pH is increased (pH > pK) branching of the single file cycle occurs and new cycles appear in the flux diagrams. The branches include configurations with fewer protons (more faults) and lead to an increase in the flux. At extreme high pH's a single cycle appears again in which only a single proton is in the conductor at a time. After the proton enters the chain, it is conducted by an alternating series of jumps and group rotations. The flux is then approximately $J \simeq K_P^a \phi$ where $\phi = K(0 \leftarrow \mathrm{L_r})/(K(0 \leftarrow \mathrm{L_r}) + K_D^a)$. $K_{P,D}^a$ are the protonation and deprotonation rate constants at side a. Although K_P is essentially independent of pH at basic pH's, $K_D(\mathrm{XH})$ increases with increasing pH so that $\phi \to 0$ and the flux vanishes.

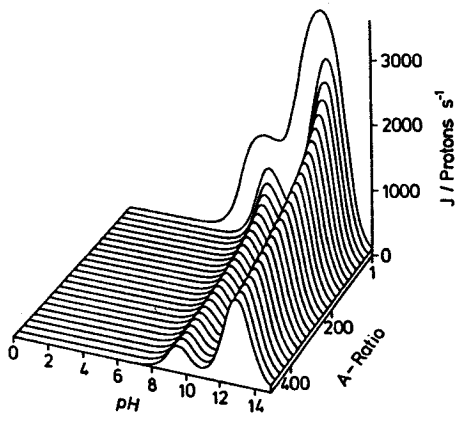

Fig. 6. Dependence of the stationary proton current on the rate constants for group rotation for a system in Fig. 3 with pK(XH) = 10; the frequency factor A_{ij} for group rotations in Eq. (2.2) is multiplied by the factor A-Ratio. The current has been rescaled by $1/A$-Ratio

In Fig. 6 we have examined the effect of speeding up the rotational rate constants by multiplying the frequency factor A_{ij} for all rotations of the groups by a factor A-Ratio. At A-Ratio = 500 the migration of a rotational fault is approximately as fast as the jump process. The curve for A-Ratio = 1 is just a cross-section of Fig. 3 with pK = 10. The current for A-Ratio > 1 has been rescaled by the factor $1/A$-Ratio to simplify the comparison. For pH < pK = 10, the protons are conducted by the L_t-L_r single file cycle discussed earlier. At low pH's (A-Ratio = 1) the flux is primarily determined by the deprotonation at side b which is extremely slow, so that accelerating the rotations of the conductor groups should have no influence on the proton flux. Whereas the flux at the first plateau for A-Ratio = 1 is primarily determined by the formation of a Bjerrum rotational fault, for A-Ratio = 500 the plateau develops into a maximum, the height depending on the deprotonation rate $K_D(\mathrm{XH})$. The flux is now considerably larger; for example, at pH = 9 one finds for A-Ratio = 500 a current of $1.085 \cdot 10^5$ protons s^{-1} whereas for A-Ratio = 1 the current measures only $1.689 \cdot 10^3$ protons s^{-1}. The deprotonation rate and hence, the current increase with increasing pH until at pH = 10, K_D is equal to the constant to create a Bjerrum L_r fault which then limits the current.

We consider now proton conductors composed of side groups able to accept two protons (D_t faults), e.g. a chain of serines. To reflect the difficulty in maintaining the second proton on the side group, we have chosen $\mathrm{pK}(\mathrm{XH_2})$ negative, $\mathrm{pK}(\mathrm{XH_2}) = -2$. With this pK-value, the excess proton (D_t fault) has a lifetime in the conductor on the scale of the jump process ($\simeq 10^{-10}$s) since deprotonation at the end groups is extremely fast ($K_D(\mathrm{XH_2})$

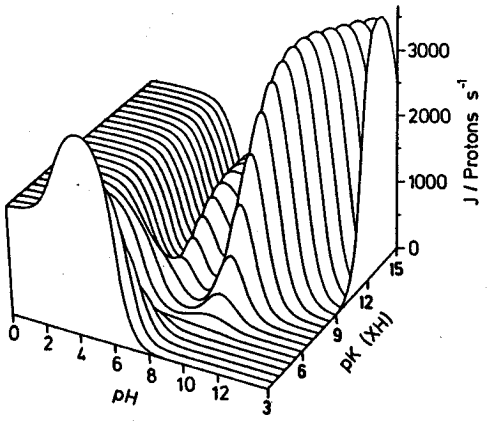

Fig. 7. Stationary proton current across a homogeneous chain of $N = 4$ side groups capable of accepting two protons as a function of pK(XH) with $pK(XH_2) = -2$ fixed and as a function of $pH = pH_a = pH_b$. The current is induced by an external electrical potential, $\Delta V_{ext} = 100\,mV$

$\simeq 10^{12} s^{-1}$). Holding the $pK(XH_2)$ value constant, we have determined numerically the stationary current induced by a fixed voltage of 100 mV. Figure 7 presents this proton current as a function of pK(XH) and the solution pH. At basic pH's, Figs. 3 and 7 are practically identical, for example the same configurations and cycles are involved in the transport. At acidic pH's the ability of the groups to accept an additional proton opens up a new pathway, and the transport now consists of two single file cycles shown in Fig. 4. The lower (and the principal) pathway conducts by introducing an excess proton (D_t fault) into the conductor. After the proton migrates across the chain and is released into the solution, the conductor returns to its original configuration by rotations of the side groups. The free energy diagram for the $D_t - L_r$ cycle for pK = 12 and pH = 6 is shown in Fig. 5b. Effective rate constants of the condensed translations of the D_t fault $k_{\pm 3}$ can be calculated as in the previous example for the $(L_t - L_r)$ translational-rotational cycle,

$$k_{+3} = K_P^a(XH)\,\phi\,\frac{1-s}{1-s^3}$$
$$k_{-3} = K_P^b(XH)\,\phi'\,\frac{1-s^{-1}}{1-s^{-3}} \qquad (3.16)$$

where $\phi\,(\phi')$ is a measure of the efficiency of the protonation step

$$\phi(\phi') = \frac{K(D_t \rightleftarrows D_t)}{K_D^{a(b)}(XH_2) + K(D_t \rightleftarrows D_t)}$$

The third factor in (3.16) is an analogous gambler's ruin expression for the motion of the D_t fault. The applied voltage gives rise to a bias

$$s = \exp(-\beta\mu_t \Delta V_{ext}/d). \qquad (3.17)$$

The total flux J is estimated from the reduced cycle

$$A \underset{k_{-1}}{\overset{k_1}{\rightleftarrows}} B \underset{k_{-2}+k_{-3}}{\overset{k_2+k_3}{\rightleftarrows}} A \qquad (3.18)$$

according to (3.12) and (3.15). For pK = 12 and pH = 6, the effective rates are $k_3 = 378.3\,s^{-1}$ and $k_{-3} = 41.50\,s^{-1}$, and the proton current through the combined cycles is 361 protons s^{-1} of which the $D_t - L_r$ cycle contributes 244 protons s^{-1} and the $L_t - L_r$ cycle 117 protons s^{-1}. The approximate value agrees with the numerical calculations in Fig. 7 within 1%.

For either of the simple unbranched single file mechanisms treated above a rather complex expression for the stationary proton current can be obtained directly from the kinetic equations as shown by Nagle *et al.* [7]. In the special case that the rate constant for deprotonation of the end group is the same as that for the internal proton translation these authors provide an analytical expression for the flux which is similar to (3.15).

3.3. Linear voltage-current relationship

At small chemiosmotic potential differences between the conductor end groups a and b, i.e. small electrical potentials ΔV_{ext}, small pH-differences, or a combination of the two, the conductor operates near thermal equilibrium and a linear relationship between the proton current J and the generalized thermodynamic force (affinity) should exist. In the absence of a pH-difference $\mathcal{A} = e\beta\Delta V_{ext}$. The affinity for a single step $i \rightarrow i+1$ in the transport cycle is

$$\mathcal{A}_i = \ln \frac{K_{i+1i} P_i}{K_{ii+1} P_{i+1}}. \qquad (3.19)$$

For an unbranched cycle with vertices (configurations) ordered, $i = 1,2, \ldots M$, the total affinity is

$$\mathcal{A} = \sum_{i=1}^{M} \mathcal{A}_i = e\beta\Delta V_{ext}. \qquad (3.20)$$

At small applied voltages one may linearly expand the rate constants and distributions in (3.19); $K_{ii+1} = K^\circ_{ii+1}(1+\delta_i)$, $K_{i+1i} = K^\circ_{i+1i}(1+\delta_i)$, $P_i = P_i^\circ(1+\varepsilon_i)$, $P_{i+1} = P^\circ_{i+1}\ (1+\varepsilon_{i+1})$. The affinity for the transition $i \rightarrow j = i+1$ can be approximated by

$$\mathcal{A}_i \simeq \ln \frac{K^\circ_{ii} P_i^\circ}{K^\circ_{ij} P_j^\circ} + \ln \frac{1+\delta_i}{1+\delta_i} + \ln \frac{1+\varepsilon_i}{1+\varepsilon_j}. \qquad (3.21)$$

Since the equilibrium distribution satisfies detailed balance, i.e. $K^{\circ}_{ji}P^{\circ}_i = K^{\circ}_{ij}P^{\circ}_j$, one obtains

$$\mathscr{A}_i \simeq \delta_i - \bar{\delta}_i + \varepsilon_i - \varepsilon_j . \tag{3.22}$$

The flux at the transition $i \rightarrow j$, $F_{ij} = K_{ji}P_i - K_{ij}P_j$ can be similarly simplified

$$F_{ij} \simeq K^{\circ}_{ji}P^{\circ}_i(\delta_i - \bar{\delta}_i + \varepsilon_i - \varepsilon_j) . \tag{3.23}$$

However, in the stationary state and for a linear cycle, the fluxes F_{ij} are all equal to the proton current J, and a comparison of (3.23) and (3.22) yields

$$\mathscr{A}_i = J/(K^{\circ}_{ji}P^{\circ}_i) . \tag{3.24}$$

The desired linear voltage-current relationship follows from (3.20)

$$\Delta V_{ext} = R\,J$$

with

$$R = \sum_{i=1}^{M} kT/e(K^{\circ}_{i+1\,i}P^{\circ}_i) . \tag{3.25}$$

R represents the resistance of the conductor. This derivation is a generalization of the one given by Schnakenberg [14] in that the essential deviations of K°_{ij} from K_{ij} are included.

Branched cycles can be treated as in the theory of electrical networks. For example, a 2-cycle diagram such as in Fig. 4 corresponds to the diagram

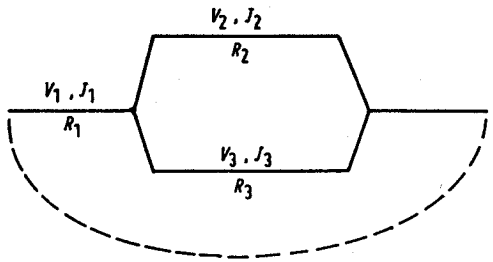

(3.26)

For each unbranched segment, (3.25) holds, i.e. $V_i = R_iJ_i$, $i = 1,2,3$. Kirchoff's rules apply

$$J = J_1 = J_2 + J_3;\ V_2 = V_3;\ \Delta V_{ext} = V_1 + V_2$$

and yield

$$\Delta V_{ext} = \left[R_1 + \left(\frac{1}{R_2} + \frac{1}{R_3} \right)^{-1} \right] J. \tag{3.27}$$

In Fig. 8 we compare at three different pH-values the proton current evaluated numerically from the general master equation to that obtained from the linear approximation around thermal equilibrium (3.27). The

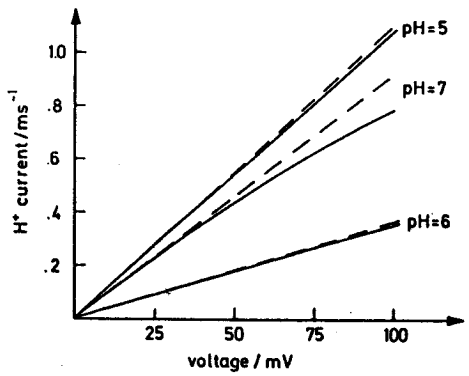

Fig. 8. Applied voltage-current relationship for the proton current through a conductor from Fig. 7 with pK(XH) = 10: (——) are the currents evaluated numerically, (– – –) are the currents evaluated from approximations (3.25) and (3.27)

transport involves i) at pH = 5, the $D_t - L_r$ single file cycle, ii) at pH = 6, the branched D_t, $L_t - L_r$ single file cycles, and iii) at pH = 7, the $L_t - L_r$ single file cycle. In all cases the linear relationship is satisfed with good accuracy. For each linear (unbranched) cycle, the total resistance R can be divided into a contribution proportional to the length N of the conductor and a contribution independent of N

$$R = R_c + N(R_r + R_t). \tag{3.28}$$

R_c can be interpreted as a contact resistance arising from the protonation and rotation of the end groups which depends on pH. R_r and R_t are specific resistances that characterize the motion of the L_r rotational and of the L_t or D_t translational faults, respectively.

3.4. Transport in heterogeneous conductors

Proton conduction across energy tranducing membranes often has a distinct vectorial character. Hence, the corresponding components in the membrane would function best if the underlying proton conductors obey a diodic voltage-current characteristic. An example of such a component is the light-driven proton pump bacteriorhodopsin which should have a low proton resistance in the extracellular direction and a high resistance in the cytoplasmic direction. That such diodic property can be realized by hydrogen-bridged chains of amino acid side groups will be demonstrated here. To achieve this property the proton conductor has to be necessarily heterogeneous. The heterogeneity can be achieved by the alignment of hetero-

geneous (acidic and basic) side groups, by the presence of internal electric fields, or by a combination of the two. We consider first proton diodes composed of acidic and basic side groups and then proton diodes realized solely by internal electric fields.

Figure 9a shows the stationary proton current across a conductor composed of two acidic (A) and two basic (B) side groups as a function of the applied voltage ΔV_{ext} and solution pH. In the following text this heterogeneous conductor will be referred to as the AB diode. The groups are characterized by the pK values

	A	A	B	B
pK(XH)	4	4	17	17
$pK(XH_2)$	−2	−2	9	9 .

The pK value of the basic side group, $pK(BH_2) = 9$, is typical for lysine, and the pK value of the acidic side group, $pK(AH) = 4$, is typical of aspartic or glutamic acid. Since titration curves reveal that the amino acid side groups are normally only able to accept or give up a single proton, the second pK value of the basic (acidic) groups, $pK(BH) = 17$ ($pK(AH_2) = -2$), were chosen to be large (small). We note that the rate constants for the transport of a proton across the A−B junction given in Table 1 are distinct from those between homogeneous groups. In particular by increasing the value of E_{LD} we have assumed that the formation of a double ionic fault ($D_t^B L_t^A$) between heterogeneous groups is as fast, but much more stable than the formation of one between identical groups.

As seen in Fig. 9a, the maximum current across the AB diode occurs for positive voltages when the solution pH is neutral. The Φ_c graph of the cycles involved in the forward proton current for pH = 7.5 and $100\,mV < \Delta V_{ext} < 400\,mV$ is shown in Fig. 9b. The numbers indicate the current through the various cycles at $\Delta V_{ext} = 250\,mV$. All the cycles in Fig. 9b involve the transition $T_{A\to B}$ whereby a proton jumps from the acid to the basic group (AH BH → A HBH). The greater stability of the latter configuration gives rise to the vectorial transport of the proton. The reverse current is determined by the rate constant for this transition in the reverse direction. The greater the pK difference, $pK(BH_2) - pK(AH)$, the more severely the reverse transport is blocked. Large pK differences lead, however, to compensating effects arising from the (de-)protonation of the end groups, i.e. reduction of the forward current. To mitigate this effect and promote the efficiency of the heterogeneous diode, we have taken the (de-)protonation rate constants to be field dependent as given in (2.6). Similarly the choice of E_{LD} in Table 1 allows the reverse current to be blocked without resorting to components with extreme pK differences.

The free energy diagrams (not presented here) of the cycles in Fig. 9b show that the forward proton current is controlled by three processes:

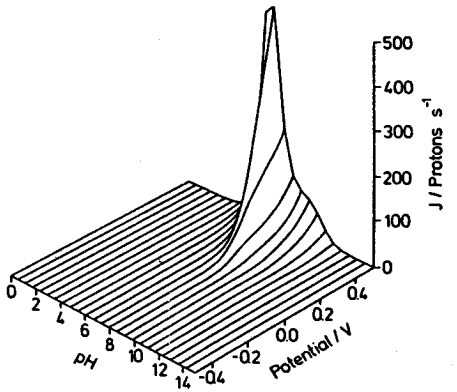

Fig. 9. a) Electrical voltage induced stationary proton current across an AB-diode as a function of applied voltage and solution pH ($pH = pH_a = pH_b$). The pK values of the diode components are provided in the text

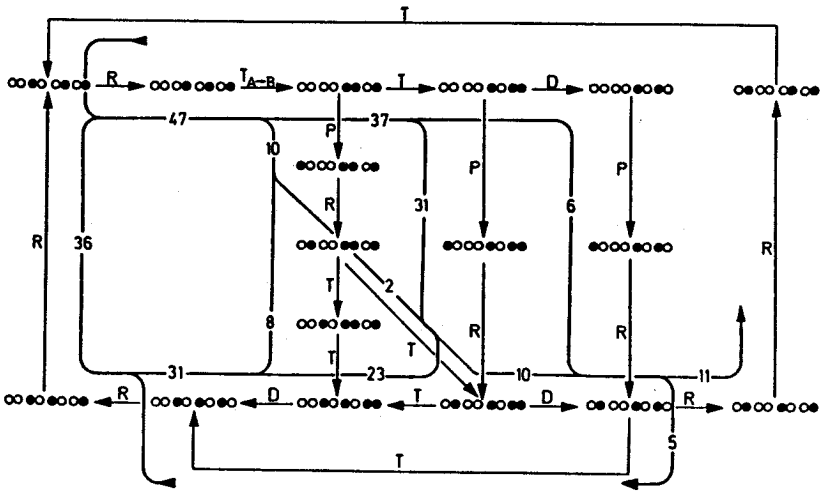

Fig. 9. b) The Φ_c-graph of the conduction pathways in the AB-diode at pH = 7.5 and 100 mV $< \Delta V_{ext} <$ 400 mV. The transition fluxes for $\Delta V_{ext} = 250\,mV$ are indicated along the transitions

protonation of the end groups and formation of an L_r fault. The slowest step is the protonation of the acidic group. The corresponding rate constant at 100 mV is $K_P(A) = 636\,s^{-1}$ and increases slowly with the applied voltage. Deprotonation and formation of an L_r rotational fault at the basic end group are both about 10 times faster. After releasing a proton to the solution, the yield ϕ of the subsequent conduction sequence depends on whether

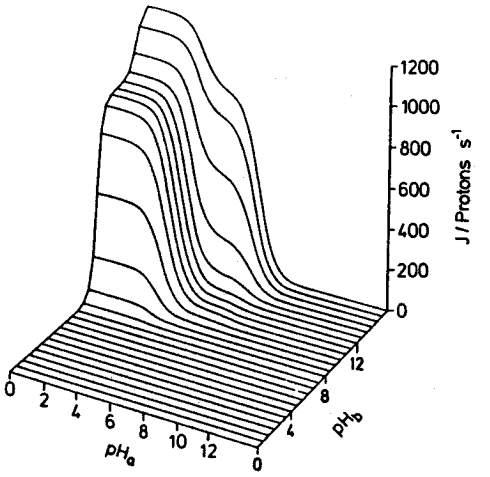

Fig. 10. Stationary proton current across the AB-diode of Fig. 9 induced by a pH gradient

the end group can rotate faster than it is reprotonated, the yield being then $\phi = K(L_r \leftarrow 0)/[K(L_r \leftarrow 0) + K_P(BH)]$. $K_P(BH)$ decreases and $K(L_r \leftarrow 0)$ increases with increasing voltage and one determines at 100 mV, $\phi = 4 \cdot 10^{-2}$ and at 400 mV, $\phi = 4 \cdot 10^{-1}$.

In Fig. 10 the proton current across the AB diode is induced by a chemical potential difference, i.e. different solution pH's on the acidic side (pH_a) and the basic side (pH_b). A strong forward current occurs when pH_b is large and pH_a is small. In the plateau region at $0 < pH_a < 3$ and $11 < pH_b < 13$, protons are conducted by the single file cycle involving D_t and L_r faults (bottom of Fig. 4). In this region the protonation of the acidic end group is so fast that the forward proton current is completely determined by the rotations of the groups. Reducing the $D_t - L_r$ cycle as in Section 3.2, one can estimate the current by use of Eq. (3.8a) with $s = 1$ and $N = 4$ to obtain

$$J \simeq \lim_{s \to 1} K(L_r \leftarrow 0) \frac{s-1}{s^4-1} = K(L_r \leftarrow 0)/4 = 920 \text{ protons s}^{-1}$$

in good agreement with the numerical value in Fig. 10.

A reversal of the pH_a and pH_b values, i.e. $pH_a > pH_b$, leads to a very small proton current. Hence, the AB diode assumes diodic properties for electrical (Fig. 9) as well as for chemical potentials (Fig. 10). The diodic character is achieved by the translation of the excess proton from the acidic to the basic group in the transition HAH BH → HA HBH. The back transition is extremely slow since the configuration with a D_t fault on a basic group is much more stable than the configuration with the fault on an acidic group, $pK(BH_2) \gg pK(AH_2)$.

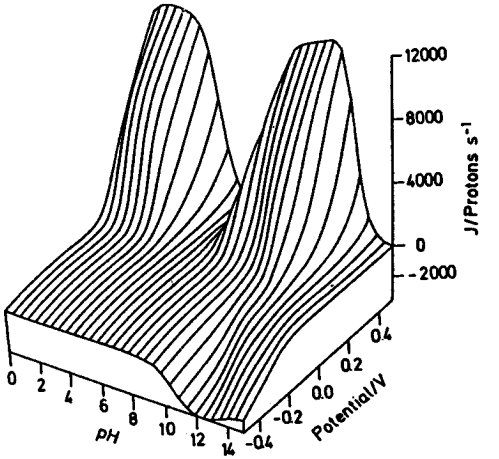

Fig. 11. Electrical voltage-induced stationary proton current across a field diode as a function of the applied voltage and solution pH [$pH = pH_a = pH_b$, $N = 4$, $pK(XH) = 10$, $pK(XH_2) = -2$, $\Delta V_{int} = -300$ mV]

A proton diode can also be constructed from a homogeneous chain by the presence of an appropriate internal field. The internal field can arise through dipoles aligned along the conductor. Edmonds [13] has suggested that a water channel spanning a biomembrane could conduct ions vectorially if the dipoles of the water molecules were properly oriented. Proton transporting proteins could achieve an internal electric field by the dipole moments of oriented polar side groups and/or the dipole moments of the backbone. To this point it is of interest to observe that bacteriorhodopsin is composed of seven α-helices spanning the outer membrane of H.h. Since consecutive α-helices are oppositely directed one excepts that the dipole moments of six α-helices cancel and the dipole moment of a seventh helix remains. Since the NH-terminal end is located at the extracellular side the diodic current would be directed outside → inside, i.e. opposite to the pump direction. This may be in harmony with the observation that the initial charge displacement in bacteriorhodopsin is against the pump direction.

The stationary proton current along a homogeneous chain with an internal field as a function of the applied voltage and of the solution pH is shown in Fig. 11. The chain consists of side groups able to accept two protons, the corresponding pK-values for the different protonated species being $pK(XH_2) = -2$ and $pK(XH) = 10$. The internal field assumed is linear with a zig-zag profile, the free energy being 150 mV above the solution at the *a* side, falling off linearly by 300 mV with a free energy 150 mV below the solution at side *b*. The strength of the internal field, 300 mV, is a typical value obtained in calculations of the electrostatic potential of α-helical proteins [20].

Figure 11 demonstrates that the conductor described has a diodic voltage-current characteristic in that it gives rise to a larger proton current in one direction than in the reverse direction. This conductor will be referred to as the "field diode" in the following text. The diodic characteristic of the field diode is realized over a larger pH range with a stronger current than in the case of the AB diode. This broadening is due to the more favourable conditions for (de-)protonation at the end groups. The internal field of $\Delta V_{int} = 300\,mV$ modifies the pK values so that the end group at side *a* (left) has the effective pK values, $pK^a(XH) = 7.46$, $pK^a(XH_2) = 4.53$ and the end group at side *b* (right) the effective values, $pK^b(XH) = 12.53$, $pK^b(XH_2) = 0.53$. However, around neutral pH values the current decreases from a maximum value of about 10^4 protons s^{-1} to $2.5 \cdot 10^2$ protons s^{-1} at $\Delta V_{ext} = 400\,mV$. This reduction occurs when due to a retardation of the $O \rightarrow D_t$ process the diode switches from a $D_t - L_r$ single file mechanism to an $L_t - L_r$ single file mechanism.

At relatively low voltages, $-200\,mV < \Delta V_{ext} < 200\,mV$ and neutral to slightly basic pH's, the proton conduction in the Φ_ε-flux diagrams consists principally of the single file cycle involving the motion of an L_t negative ionic fault (hole) and a rotational L_r fault (see top of Fig. 4). The free energy profiles for the forward and reverse currents at $\Delta V_{ext} = \pm 200\,mV$ are sketched in Fig. 12. In the forward direction, the internal and external fields are both accelerating the rotation and translation steps whereas in the reverse direction the external field opposes the internal field. At a reverse voltage of $\Delta V_{ext} = -200\,mV$, the protons still have to overcome a considerable bias in the conduction pathway. At $\Delta V_{ext} = \Delta V_{int} = -500\,mV$, the activation barriers for the rotations and translations in Fig. 12b become symmetrical which leads to a larger reverse current as shown in Fig. 11.

The free energy profiles for the forward direction (Fig. 12a) shows that three processes play an almost equal role in determining the proton current: (1) the rotation of the end group to introduce an L_r fault into the conductor and its subsequent migration across the conductor; (2) deprotonation on one end and the subsequent migration of the L_t fault; (3) reprotonation at the other end. The single file cycle can be replaced by a three component reduced cycle as indicated in the diagram. The effective rotational rate constants $k_{\pm 1}$ are approximated by the gambler's ruin expressions (3.8) and (3.10). The bias ratio s_r in this case is

$$s_r = \exp\,[-\beta\mu_r(\Delta V_{ext} f - \Delta V_{int})/d].$$

The translation steps are so strongly biased in the forward direction that the effective forward rate constant k_{+2} is taken to be just the field-dependent deprotonation rate constant given by (2.6)

$$k_{+2} = K_D^b(XH) = = 2 \cdot 10^{10}[10^{-pK-\Delta pK} - 10^{pH-14}].$$

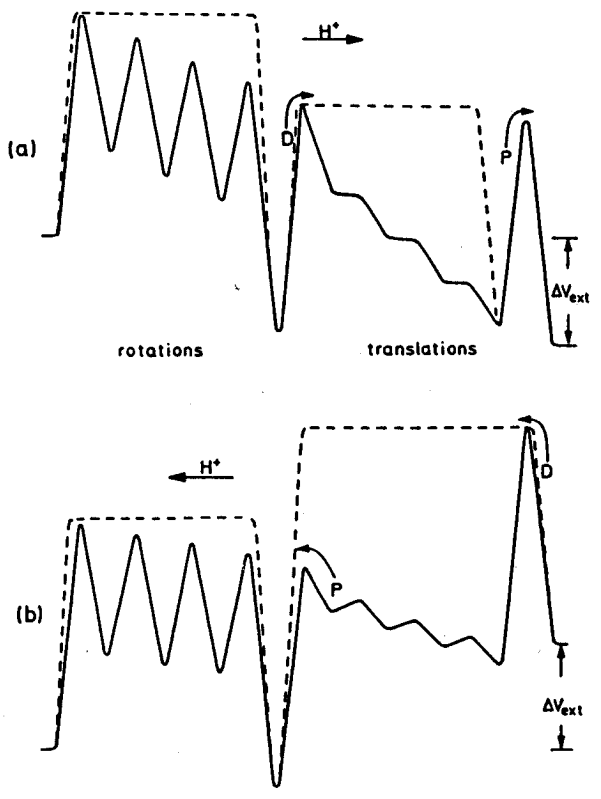

Fig. 12. Free energy profiles of the $(L_t - L_r)$ single file transport cycle for the field diode in Fig. 11: a) at an applied forward voltage $\Delta V_{ext} = 200\,mV$; b) at an applied reverse voltage $\Delta V_{ext} = -200\,mV$. The dotted lines indicate the reduced representation of the single file cycles discussed in the text. The solution is at pH = 7.5

The effective rate constant for the reverse process k_{-2} can be calculated from the consistency condition

$$\frac{k_{+2}}{k_{-2}} = \frac{K_D^b}{K_P^b} s_t^{-N+1}$$

with the bias ratio s_t

$$s_t = \exp\,[-\beta\mu_t(\Delta V_{ext} f - \Delta V_{int})/d].$$

It follows that

$$k_{-2} = K_P^b s_t^{N-1}.$$

The effective rate constants $k_{\pm 3}$ are just the field dependent protonation and deprotonation rate constants at side a obtained from (2.6)

$$k_{+3} = K_P^a(\mathrm{X})$$

$$k_{-3} = K_D^a(\mathrm{XH})\,.$$

Since s_r is so small in the forward direction that $k_{-1} \sim 0$, it is sufficient to consider the reduced cycle

$$A \xrightarrow{k_1} B \underset{k_{-2}}{\overset{k_2}{\rightleftharpoons}} C \underset{k_{-3}}{\overset{k_3}{\rightleftharpoons}} A\,. \tag{3.29}$$

The flux is estimated by solving exactly the rate equations for the above reduced cycle

$$\begin{aligned} J^{-1} &= \frac{1}{k_1}\left[1 + \frac{k_{-3}}{k_{+3}}\left(1 + \frac{k_{-2}}{k_{+2}}\right)\right] + \frac{1}{k_3}\left(1 + \frac{k_{-2}}{k_{+2}}\right) + \frac{1}{k_{+2}} \\ &= \frac{1}{k_1}\left[1 + 10^{\mathrm{pH}-\mathrm{pK}-\Delta\mathrm{pK}}\,(1 + s_t^{N-1}\,10^{-\mathrm{pH}+\mathrm{pK}-\Delta\mathrm{pK}})\right] \\ &\quad + \frac{1}{K_P^a}\,(1 + s_t^{N-1}\,10^{-\mathrm{pH}+\mathrm{pK}-\Delta\mathrm{pK}}) + \frac{1}{K_D^b}\,. \end{aligned} \tag{3.30}$$

For the conditions in Fig. 12a, pH = 7.5 and $\Delta V_{\mathrm{ext}} = 200\,\mathrm{mV}$, we obtain from (3.30), $J = 2.1$ protons ms^{-1} in comparision with the exact numerical value $J = 2.3$ protons ms^{-1} of Fig. 11. An approximation to the reverse current can be calculated by performing the reduction indicated in Fig. 12b.

At acidic pH's the primary pathway in the forward direction is a single file cycle with D_t and L_r faults (Fig. 4 bottom). The proton current can be approximated by an expression similar to (3.30). At large positive voltages, the maximum current is limited by the formation of the L_r rotational fault, e.g. at pH = 2 and $\Delta V_{\mathrm{ext}} = 400\,\mathrm{mV}$, $K(\mathrm{L_r} \leftarrow 0) = 1.12 \cdot 10^4\ \mathrm{s}^{-1}$ and $J = 9.84 \cdot 10^3$ protons s^{-1}.

At basic pH's and large reverse voltages, the single file mechanism in Fig. 12b no longer applies. The rate of deprotonation $K_D^a(\mathrm{XH})$ is much larger than the rate of migration of a rotational L_r fault, so that after the end group rotates to introduce the L_r fault into the conductor, the end group is immediately deprotonated. The reverse current increases appreciably because several new and branched conduction pathways containing simultaneously L_t and L_r faults now exist.

Figure 13 shows that a proton current across the field diode can also be induced by a pH gradient. Like the AB diode, the maximum current in this case is limited by a rotation of the end group to create an L_r fault. The cycles participating in the transport are more complex than those contributing to the current in Fig. 11. The vectorial character of a field diode conducting in

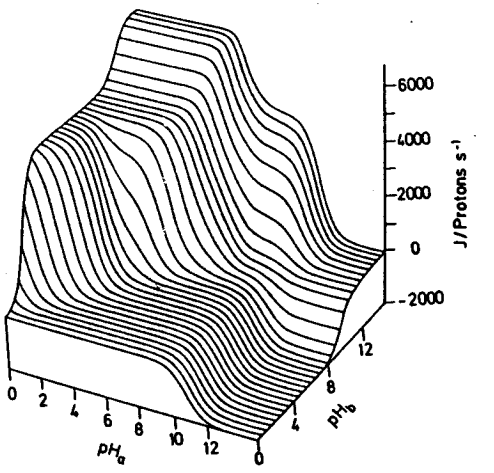

Fig. 13. Stationary proton current across the field diode in Fig. 11 induced by a pH gradient

the pH gradient (chemical potential) mode of Fig. 13 is less developed than in the electrical potential mode of Fig. 11 since in the former only the deprotonation and protonation rates are accelerated.

4. Relaxation of a proton conductor after proton injection or ejection — strong transfer model

In Sections 4 and 5 we examine the relaxation of a proton conductor after the injection of a proton at the end group or after ejection (abstraction) of a proton from the end group. The end group could be, for example, one of the amino acid side groups of bacteriorhodopsin that receives a proton from the chromophore after it has been photochemically activated. To simplify the analysis, we consider first a model in which a very acidic (basic) group protonates (deprotonates) instantaneously at time $t = 0$ the left end group of a conductor assumed to be in thermal equilibrium with the right end in contact with a proton reservoir. Obviously only those configurations i of the conductor can become protonated (deprotonated) which contribute to the equilibrium and offer an empty (a filled) protonation site at the left most position. Direct reversal of the injection (ejection) process at times $t < 0$ is not allowed, i.e. the proton injected (the hole) is forced to leave the conductor at the opposite end. This prototype injection (ejection) model corresponds to a very acid (basic) group which donates the proton (hole) very fast. In Section 5 we replace this model by a more realistic and complex situation.

To characterize the relaxation of the conductor we choose four observables which are suggested by recent experimental investigations. These

observables are 1) changes in the conductor's dipole moment; 2) changes in the free energy; 3) the integrated proton current; and 4) the state of protonation of any group along the conductor. For bacteriorhodopsin measurements of these observables during the pump cycle have already been performed in part. In particular, the time dependence of the charge displacements (dipole moments) has been shown to exhibit two relaxation times [21]. Ort and Parson [22] and Caplan [23] have made photo-acoustical measurements of the enthalpy changes. The appearance of a proton and a hole conducted through bacteriorhodopsin after light excitation has been observed by several groups [3]. Hess and Kuschmitz [24] have observed a deprotonation-protonation process at a group distant from the photochemically active chromophore.

4.1. Time-dependent solution

The relaxation of the conductor after injection (ejection) of a proton at the left-hand end group is described by

$$\dot{P}(t) = \mathbf{K}^{inj} P(t) \tag{4.1}$$

where

$$K_{ij}^{inj} = \begin{cases} 0 & \text{for } j \to i \text{ corresponding to (de-)protonation at the left end,} \\ K_{ij} & \text{otherwise as in Section 2.} \end{cases}$$

Before the proton is injected (ejected) we assume the system is in equilibrium so that the initial distribution $P(0)$ is

$$P(0) = P^\circ + \Sigma P_i^\circ \, (e_j - e_i). \tag{4.2}$$

$(i \to j)$ (de-)protonation at the left end

P° is the equilibrium distribution satisfying

$$\mathbf{K}^{inj} P^\circ = 0. \tag{4.3}$$

e_i is the unit vector for the i-th proton configuration. The second term describes the redistribution of the contributions from configurations involving (de-)protonation at the left-hand side.

The probability for the injection (ejection) of a proton is

$$I(P^\circ) = \Sigma P_i^\circ. \tag{4.4}$$

$(i \to j)$ (de-)protonation at the left end

The injection probability $I(P^\circ)$ is greater the more likely the leftmost protonation site is unfilled in P°. For example, it would be easier to inject a proton when the right end is in contact with a basic solution than with an acidic solution.

The master Eq. (4.1) with the initial condition (4.2) has the formal solution

$$P(t) = \exp(t \, \mathbf{K}^{inj}) \, P(0). \tag{4.5}$$

The matrix $\mathbf{K}^{inj}$ can be symmetrized by the following similarity transformation S

$$\begin{aligned} S_1 &= 1.0 \\ S_i &= S_j \sqrt{K_{ij}^{inj}/K_{ji}^{inj}} \quad \text{for} \quad K_{ji}^{inj} \neq 0. \end{aligned} \tag{4.6}$$

S is well-defined because the elements of the rate matrix $\mathbf{K}^{inj}$ obey a detailed balance condition.

After the injection (ejection) of a proton, it is convenient to characterize the deprotonation (protonation) at the solution side by the integral of the proton current

$$T_R(t) = \begin{cases} \int_0^t \mathrm{d}t' \, J_R(t') & \text{injection} \\ \int_0^t \mathrm{d}t' \, J_R(t') + I(P^\circ) & \text{ejection} \end{cases} \tag{4.7}$$

$J_R(t)$ is calculated as in the stationary case in Section 3. Asymptotically $T_R(t)$ equals the injection probability (4.4),

$$\begin{aligned} T_R(0) &= \begin{cases} 0 & \text{injection} \\ I(P^\circ) & \text{ejection} \end{cases} \\ T_R(\infty) &= \begin{cases} I(P^\circ) & \text{injection} \\ 0 & \text{ejection} \end{cases} \end{aligned} \tag{4.8}$$

Condition (4.8) was used as a non-trivial test for the stability of the calculations.

As a measure of the system's deviation from equilibrium, we also evaluated the change in its free energy

$$\Delta F(t) = kT \sum_i \mathrm{P}_i(t) \ln ((P_i(t)/P_i^\circ) \tag{4.9}$$

where P_i° are components of the equilibrium distribution defined in (4.3). Expressing P_i° in terms of the internal energy U_i of the i-th configuration and the partition function Z, we can re-write (4.9)

$$\begin{aligned} \Delta F(t) &= kT \sum_i (t) \ln P_i(t) - kT \sum_i P_i(t) \ln (Z^{-1} \, e^{-U_i/kT}) \\ &= -TS(t) + \sum_i U_i P_i(t) + kT \ln Z \\ &= -TS(t) + E(t) - F_0 \\ &= F(t) - F_0. \end{aligned}$$

$E(t)$ is the internal energy, $S(t)$ the entropy, and $F(t)$ the free energy of the system at time t. $F_0 = -kT \ln Z$ is the free energy of the equilibrium distribution. In [14] it was shown that $\Delta F(t)$ is a Liapunov function that monotically decreases with time.

The dipole moment of the conductor is given by

$$\mu(t) = \sum_i \mu_i P_i(t) + ed\, T_R(t). \tag{4.10}$$

μ_i is the dipole moment of the i-th configuration and is defined as the sum of the dipole moments of all protons in the i-th configuration with the reference point taken at the left-hand side,

$$\mu_i = \sum_{\alpha \in C_i} [\mu_r n_r(\alpha) + \mu_t n_t(\alpha)]. \tag{4.11}$$

$n_r(\alpha)$ $[n_t(\alpha)]$ is the number of rotations (translations) necessary to bring the proton from the left side to position α. The summation in (4.11) is restricted to the set of positions C_i occurring in the configuration i. The deprotonation (reprotonation) at the solution side contributes the second term in (4.10). Asymptotically the fraction $I(P^\circ)$ of charge will be transported across the membrane, i.e. $\mu(\infty) - \mu(0) = ed\, I(P^\circ)$.

The state of protonation of any group j along the conductor is determined by

$$\begin{aligned} [X_j](t) &= \sum_{i \in D_0(j)} P_i(t) \\ [X_jH](t) &= \sum_{i \in D_1(j)} P_i(t) \\ [X_jH_2](t) &= \sum_{i \in D_2(j)} P_i(t) \end{aligned} \tag{4.12}$$

where $D_0(j)$ $[D_1(j), D_2(j)]$ is the set of indices of all the configurations for which the j-th group is unprotonated [singly, doubly protonated].

In order to identify the mechanisms and cycles contributing to the non-stationary proton transport, we employ again the Φ_ε-graphs introduced in Section 2, however, determined for the integrated transition fluxes

$$T_{i \to j}(\infty) = \int_0^\infty F_{i \to j}(t) \mathrm{d}t. \tag{4.13}$$

4.2. Quasi-stationary distribution

After injection (ejection), the proton distribution is considerably displaced from its equilibrium value. In returning to equilibrium the processes such as translations and, depending on the pH and pK, protonations occur, if possible, before the slower rotational motions. In such cases there exists often a time period $\tau_1 < t < \tau_2$, in which all elementary processes fall into two distinct classes: "fast" processes in quasi-equilibrium with rate constants

greater than τ_1^{-1} and "slow" processes with rate constants smaller than τ_2^{-1}. We let Ω be the set of M configurations that are connected through the "fast" processes. The quasi-stationary distribution $\tilde{P}$ obeys the equilibrium condition

$$\tilde{P}_\alpha K_{\beta\alpha} = \tilde{P}_\beta K_{\alpha\beta} \quad \alpha, \beta \in \Omega \tag{4.14}$$

where $K_{\alpha\beta}$ and $K_{\beta\alpha}$ are rate constants for the transition as defined in selection 2. Their normalization is obtained from the initial distribution (4.2)

$$\sum_{\alpha \in \Omega} P_\alpha = \sum_{\alpha \in \Omega} P_\alpha(0). \tag{4.15}$$

In the time period $[\tau_1, \tau_2]$ the change in the dipole moment assumes a steady value that can be approximated from (4.10)

$$\Delta\mu(\tau_1 < t < \tau_2) = \sum_{\alpha \in \Omega} \mu(\alpha)(\tilde{P}_\alpha - P_\alpha(0)) + ed\, T_R(t). \tag{4.16}$$

For the case that the transitions between the configurations in the quasi-stationary distribution form a single unbranched graph ($M = m + 1$)

$$\alpha_1 \underset{\nu_2}{\overset{\lambda_1}{\rightleftarrows}} \alpha_2 \underset{\nu_3}{\overset{\lambda_2}{\rightleftarrows}} \alpha_3 \underset{\nu_4}{\overset{\lambda_3}{\rightleftarrows}} \cdots\cdots \underset{\nu_m}{\overset{\lambda_{m-1}}{\rightleftarrows}} \alpha_m \underset{\nu_{m+1}}{\overset{\lambda_m}{\rightleftarrows}} \alpha_{m+1} \tag{4.17}$$

one can solve for the distribution explicitly,

$$\tilde{P}_i = \tilde{P}_1 \prod_{j=1}^{i-1} (\lambda_j / \nu_{j+1}). \tag{4.18}$$

The distribution has been determined with respect to the first component whose value can be obtained from the relation (4.15)

$$\tilde{P}_1 = \sum_{\alpha \in \Omega} P_\alpha(0) / \left(\sum_{k=1}^{m+1} \prod_{j=1}^{k-1} \lambda_j / \nu_{j+1} \right). \tag{4.19}$$

4.3. Mean first-passage time

The time required to establish the quasi-stationary distribution among the transitions included in (4.17) can be determined from the first-passage time approximation. To calculate the time for the configuration α_{m+1} to be reached for the first time starting from an configuration α_i, one assumes that the process $\alpha_m \to \alpha_{m+1}$ is absorbing, i.e. $\nu_{m+1} = 0$. The kinetics of the resulting stochastic processes can be described by the m-dimensional master equation

$$\dot{P}(t) = \mathbf{R}\, P(t) \tag{4.20}$$

where $P_i(t)$ is the distribution of the configuration, $i = 1,2,\ldots..m$ in Ω, and $\mathbf{R}$ is a tridiagonal matrix containing the rate constant appearing in (4.17) with $\nu_{m+1} = 0$.

A measure for the relaxation of the configuration probabilities is given by the particle correlation function $N(t)$

$$N(t) = E \cdot P(t) = \sum_{i=1}^{m} P_i(t) \tag{4.21}$$

where $E = (1, 1, \ldots 1)$. If the system is initially at $t = 0$ in the configuration k, $N(t)$ can be expressed formally as

$$N(t) = E \cdot \exp(\mathbf{R}\, t)\, e_k \tag{4.22}$$

where e_k is the unit vector $(e_k)_i = \delta_{ik}$. The first moment of $N(t)$ is the mean first passage time $\tau_{k \to m+1}$

$$\tau_{k \to m+1} = \int_0^\infty \mathrm{d}t\, N(t) = -E\, \mathbf{R}^{-1} e_k\,. \tag{4.23}$$

Due to the special form of $\mathbf{R}$, the inverse $Y^k = \mathbf{R}^{-1} e_k$ can be evaluated explicitly from the algebraic equation $\mathbf{R}\, Y^k = e_k$

$$\begin{aligned} -\lambda_1 Y_1^k + \nu_2 Y_2^k &= \delta_{1k} \\ \lambda_{j-1} Y_{j-1}^k - (\lambda_j + \nu_j)\, Y_j^k + \nu_{j+1}\, Y_{j+1}^k &= \delta_{jk} \\ \lambda_{m-1} Y_{m-1}^k - (\lambda_m + \nu_m) Y_m^k &= \delta_{mk}\,. \end{aligned} \tag{4.24}$$

These equations can be simplified to

$$\begin{aligned} -\lambda_j Y_j^k + \nu_{j+1} Y_{j+1}^k &= \begin{cases} 1 & j \geq k \\ 0 & \text{otherwise} \end{cases}, \quad j = 1,2,\ldots m\text{-}1 \\ -\lambda_m Y_m^k &= 1 \end{aligned}$$

which have the solution

$$Y_j^k = -\sum_{i=\max(j,k)}^{m} \frac{1}{\lambda_i} \prod_{k=j+1}^{i} \frac{\nu_k}{\lambda_{k-1}}\,. \tag{4.25}$$

Y_j^k can be expressed in terms of the quasi-stationary distribution evaluated in (4.18)

$$Y_j^k = -\sum_{i=\max(j,k)}^{m} \frac{1}{\lambda_i} \frac{\tilde{P}_j}{\tilde{P}_i}\,. \tag{4.26}$$

The mean first-passage time $\tau_{k \to m+1}$ is finally obtained

$$\begin{aligned} \tau_{k \to m+1} = -E \cdot Y^k &= \sum_{j=1}^{m} \sum_{i=\max(j,k)}^{m} \frac{1}{\lambda_i} \frac{\tilde{P}_j}{\tilde{P}_i} \\ &= \sum_{i=k}^{m} \frac{1}{\lambda_i \tilde{P}_i} \sum_{j=1}^{i} \tilde{P}_j\,. \end{aligned} \tag{4.27}$$

The stationary distribution and the mean first-passage time are completely determined by the rate constants describing the stochastic process. This result has been derived by a different method in [25]. From the form of (4.27) follows straight-forwardly the addition rule for the mean first-passage times

$$\tau_{1 \to m+1} = \tau_{1 \to k} + \tau_{k \to m+1}. \tag{4.28}$$

The mean first-passage times will provide in the following analyses an excellent estimate for the time periods characterizing the conductor's relaxation along certain pathways through the configuration space. However, in some instances the response is characterized by two and more relaxation times. We will, therefore, outline at the end of section 4.4 how the mean passage time method can be extended to cover two relaxation times. For this purpose one needs to employ the second moment of $N(t)$ which can be related to the mean first-passage times

$$\begin{aligned} \tau_{k \to m+1}^{(2)} &= \int_0^\infty dt\, t\, N(t) = E\, \mathbf{R}^{-2} e_k \\ &= E\, \mathbf{R}^{-1}\, Y^k = E\, \mathbf{R}^{-1} \sum_{i=1}^{m} Y_i^k e_i = E \sum_{i=1}^{m} Y_i^k\, Y^i \\ &= -\sum_{i=1}^{m} Y_i^k\, \tau_{i \to m+1}\,. \end{aligned} \tag{4.29}$$

4.4. Homogeneous conductor

Figure 14a shows the time dependence of the dipole moment $\Delta\mu(t)$, the integrated current $T_R(t)$, and the free energy $\Delta F(t)$ for a homogeneous conductor after injection and ejection of a proton at its left-hand side. The right-hand side is in contact with a proton reservoir at pH = 7. Since the equilibrium distribution P° is evenly divided between the two neutral configurations α_R and α_L containing no faults, i.e. $P^\circ = \frac{1}{2}$ (01010101 + 10101010) $= \frac{1}{2}(\alpha_R + \alpha_L)$, the total injection and ejection probabilities are 0.5. The observables in Fig. 14a vary monotonically and stepwise. The constant plateaus between the steps correspond to different quasi-equilibrium situations, and the position of the steps indicate the relaxation times of the system.

The Φ_ε-graphs of the integrated fluxes reveal that the relaxation involves the unbranched single file pathways which are represented by their free energy profiles in Figs. 14b,c (cf. Fig. 5). The curves in Fig. 14a can be readily understood after examination of these profiles. As shown in Fig. 14b, *injection* replaces the configuration α_R (01010101) by configuration

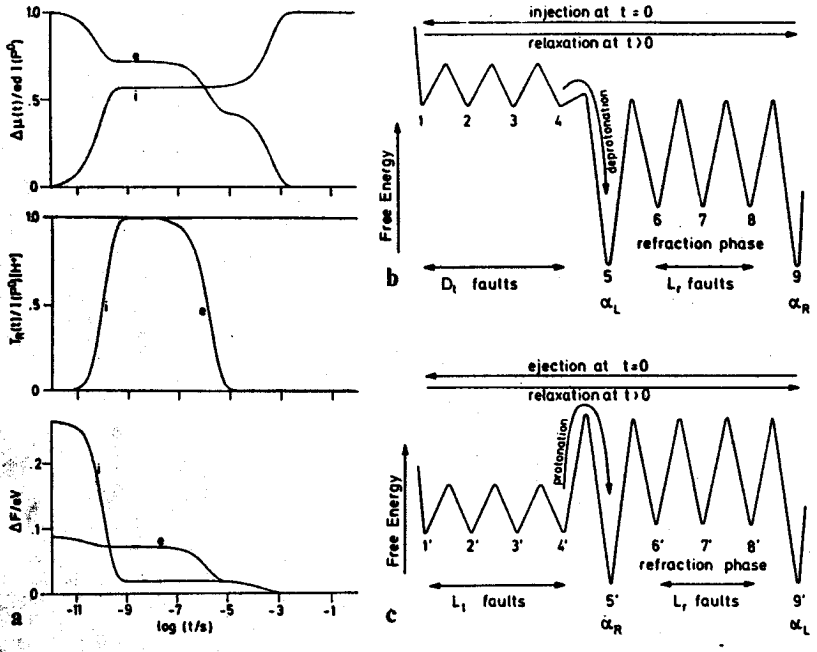

Fig. 14. a) Response of a homogeneous conductor [$N = 4$, $pK(XH) = 10$, $pK(XH_2) = -2$] after injection (i) or ejection (e) of a proton at the first group. The solution at the right is at $pH_b = 7$. Presented are the dipole moment $\Delta\mu(t) = \mu(t) - \mu(0)$ $[1 + 1\,\mu(t)/edI(P^\circ)$ for $(e)]$, the integrated proton current $T_R(t)$, and the change in free energy $\Delta F(t)$

Fig. 14. b) Free energy profile for the ($D_t - L_r$) single file pathway after proton injection. c) Free energy profile for the ($L_t - L_r$) single file pathway after proton ejection

(11010101) entailing a D_t fault at the left end. This D_t fault migrates to the right end ($\rightarrow$10101011) whereafter deprotonation leads to α_L (10101010). At this moment the conductor is in the state α_L and has still to decay to the equilibrium distribution $\frac{1}{2}(\alpha_R + \alpha_L)$. For this to happen a rotational fault must be induced at the right side by a thermal fluctuation and migrate to the left side. Figure 14c shows that *ejection* transforms the α_L (10101010) contribution to the equilibrium into configuration 1', which is an L_t fault at the left group (00101010). This fault migrates to the right reaching configuration 4' (01010100). Protonation at the right end leads to α_R (01010101). At this moment the conductor is in the state α_R and has to decay to $\frac{1}{2}(\alpha_R + \alpha_L)$ by rotation at the left side ($\alpha_R \rightarrow$ 10010101) and migration and decay of the L_r fault to the right side. For the following discussion we recall

that the energy barriers $E_A(i \rightarrow i \pm 1)$ between configurations i and $i \pm 1$ in Figs. 14b, c are related to the rate constants by $K_{ii\pm1} = 10^{13}\mathrm{s}^{-1}\exp[-\beta E_A(i \rightarrow i \pm 1)]$, i.e. provide a logarithmic measure for the rate constants.

We discuss first the behavior of the free energy change $\Delta F(t)$ in Fig. 14a since it is the observable most closely related to the free energy profiles in Fig. 14b, c. A comparison of the energy content of the configurations 1 and 1' shows that the initial free energy $\Delta F(0)$ of the injected conductor is about three times that of the ejected conductor. After injection the relaxation pathway encounters only small energy barriers (fast rates) up to the low energy equilibrium configuration 5 (α_L), and hence, one expects a fast and large decrease of $\Delta F_i(t)$. The small remaining free energy difference is due to the mixing entropy between α_L and $\frac{1}{2}(\alpha_R + \alpha_L)$ and measures only $kT\ln 2 \simeq 0.02\,\mathrm{eV}$. For this energy to decay the conductor has to overcome the rotational barriers. While the system awaits the rotation of the right end group, the conductor is in a refraction phase during which no further proton can be transported. In the case of ejection, the behavior of the conductor differs in that the free energy profile in Fig. 14c exhibits a high barrier at the protonation step 4' $\rightarrow$ 5'. One expects then that the ejected conductor first equilibrates between configurations 1',2',3', and 4' with an entropic free energy decrease of $I(P^\circ)kT\ln 4 \simeq 0.02\,\mathrm{eV}$. The free energy remains constant until protonation 4' $\rightarrow$ 5' occurs at which moment the conductor assumes the configuration α_R, i.e. its free energy approaches that of the injected conductor.

The interpretation of the free energy changes is corroborated by the time dependence of the integrated proton current $T_R(t)$ in that the current after injection and ejection coincides with the main free energy decrement, i.e. with the transitions 4 $\rightarrow$ 5 and 4' $\rightarrow$ 5'.

Figure 14a illustrates that the changes in the dipole moment are strongly correlated to the relaxation pattern of $\Delta F(t)$ and the proton current. A direct correspondence can be made between the plateau values in $\Delta\mu(t)$ and the intermediate proton configurations or quasi-equilibrium distributions. For example, after injection the conductor relaxes quickly to the configuration α_L, and hence, one expects that the plateau value of $\Delta\mu(t)$ differs from the equilibrium value $\frac{1}{2}[\mu(\alpha_L) + \mu(\alpha_R)]$ by $\Delta + edI(P^\circ)$ where $\Delta = \frac{1}{2}[\mu(\alpha_L) - \mu(\alpha_R)]$. From (4.12) one obtains

$$\mu(\alpha_L) = \frac{N(N-1)}{2}\mu_r + \frac{N(N-1)}{2}\mu_t$$

$$\mu(\alpha_R) = \frac{N(N+1)}{2}\mu_r + \frac{N(N-1)}{2}\mu_t. \qquad (4.30)$$

For $N = 4$, $\Delta = -0.43\, edI(P^\circ)$ or $\Delta\mu(t)_i = 0.57\, edI(P^\circ)$ which agrees with the value in Fig. 14a. Similarly, after ejection, one expects the second plateau in $\Delta\mu(t)_e$, associated with the state α_R, to lie by an amount $\Delta' = \frac{1}{2}[\mu(\alpha_R) - \mu(\alpha_L)]$ above the asymptotic equilibrium value. Since $\Delta' = -\Delta$, $\Delta\mu_e = 0.43\, edI(P^\circ)$ and is in agreement with Fig. 14a. To determine the early plateau value of the ejected conductor, which corresponds to the translational equilibrium between the configuration $1',2',\ldots N'$, one may employ straightforwardly the description in Section 4.2. However, in keeping with our simple arguments one expects that $\Delta\mu(t)$ differs in this early phase from the initial displacement $\mu(1')$ by the amount

$$\Delta'' = \frac{1}{N}\sum_{n'=1}^{N}[\mu(n') - \mu(1')]\, I(P^\circ). \tag{4.31}$$

With

$$\mu(n') - \mu(1') = -(n'-1)\,\mu_t \tag{4.32}$$

one determines that

$$\Delta'' = -\frac{N-1}{2}\,\mu_t\, I(P^\circ).$$

For $N = 4$, $\Delta'' = -0.29\, edI(P^\circ)$ or $\Delta\mu_e = I(P^\circ)\text{ed} + \Delta'' = 0.71\, edI(P^\circ)$ in agreement with Fig. 14a.

From our discussion it should have become clear that the steps in the curves in Fig. 14a occur whenever the conductor arrives at a new quasi-stationary state or distribution. The two steps in the relaxation behavior of $\Delta\mu(t)$ after injection correspond to the times for arrival at configurations 5 and 9. The three relaxation steps after ejection correspond to arrival at the quasi-stationary equilibrium between $1',2',3',4'$, arrival at $5'$, and arrival at $9'$. To illustrate this interpretation we provide in Table 2 the mean first

Table 2. *Mean first-passage times $\tau_{1\to j}$ for a homogeneous proton conductor after injection or ejection**

j	Injection/s	Ejection/s
2	$2.2 \cdot 10^{-11}$ (transl)	$4.7 \cdot 10^{-11}$ (transl)
3	$6.5 \cdot 10^{-11}$ (transl)	$1.4 \cdot 10^{-10}$ (transl)
4	$1.3 \cdot 10^{-11}$ (transl)	$2.8 \cdot 10^{-10}$ (transl)
5	$1.3 \cdot 10^{-11}$ (deprot)	$2.0 \cdot 10^{-6}$ (prot)
6	$2.7 \cdot 10^{-4}$ (rot)	$2.8 \cdot 10^{-4}$ (rot)
7	$5.4 \cdot 10^{-4}$ (rot)	$5.5 \cdot 10^{-4}$ (rot)
8	$8.2 \cdot 10^{-4}$ (rot)	$8.3 \cdot 10^{-4}$ (rot)
9	$1.1 \cdot 10^{-3}$ (rot)	$1.1 \cdot 10^{-3}$ (rot)

* Corresponding to the conductor in Fig. 14

passage times $\tau_{1\to j}$ for arrival at the j-th configuration in the free energy profiles in Fig. 14b, c. For example, for the case of injection, Table 2 shows that the system arrives rapidly within about 10^{-11}s at configurations 2,3,4, and 5, but then has to wait about 10^{-4}s before it passes to configurations 6,7,8, and 9. A comparison of Table 2 and Fig. 14a shows that the passage times coincide with the relaxation steps. This observation is most interesting as simple expressions for the mean first passage times can be derived from the general algorithm in Section 4.3. Using the sum rule (4.28), the first passage times in Table 2 can be expressed generally as:

$\tau_{1\to N}$	arrival at translational quasi-equilibrium
$\tau_{1\to N+1} = \tau_{1\to N} + \tau_{N\to N+1}$	deprotonation (injection) or protonation (ejection)
$\tau_{1\to N+2} = \tau_{1\to N+1} + \tau_{N+1\to N+2}$	induction of L_r fault
$\tau_{1\to 2N} = \tau_{1\to N+2} + \tau_{N+2\to 2N}$	arrival at rotational quasi-equilibrium
$\tau_{1\to 2N+1} = \tau_{1\to 2N} + \tau_{2N\to 2N+1}$	annihilation of L_r fault to reach thermal equilibrium

One obtains from (4.18) and (4.27)

$$\tau_{1\to N} = \frac{N(N-1)}{2K_t} \quad \text{where} \quad K_t = \begin{cases} K(L_t \to L_t)\ \text{ejection} \\ K(D_t \to D_t)\ \text{injection} \end{cases}$$

$$\tau_{N\to N+1} = \frac{N}{K_S} \quad \text{where} \quad K_S = \begin{cases} K_P(X)\ \text{ejection} \\ K_D(XH_2)\ \text{injection} \end{cases}$$

$$\tau_{N+1\to N+2} = \tau_{N\to N+1}\frac{K_{-S}}{K(L_r \leftarrow 0)} + \frac{1}{K(L_r \leftarrow 0)}$$

$$\tau_{N+2\to 2N} = \tau_{N+1\to N+2}(N-2) + \frac{(N-1)(N-2)}{2K(L_r \leftarrow L_r)}$$

$$\tau_{2N\to 2N+1} = \tau_{N+1\to N+2} + \frac{N-1}{K(0 \leftarrow L_r)}. \tag{4.33}$$

The simplicity of the above expressions and the excellent comparison of passage times and relaxation times in Fig. 14a demonstrate the usefulness of the mean first passage time concept. We have not clearly spelled out, however, which passage time in a cluster corresponds to the relaxation time of the variable most closely. The choice is not always straightforward. For example, we have assumed that the final relaxation process, i.e. the recovery of the conductor, ends upon reaching the last configuration $2N + 1$, 9 and $9'$

in Figs. 14b,c. Actually, the relaxation is already completed when the probability is distributed evenly between configurations $N+1$ and $2N+1$ (5 and 9 or 5′ and 9′). Therefore, $\tau_{1\to 2N+1}$ is an overestimate of the recovery time, and a better approximation would be $\tau_{1\to 3N/2+1}$, the time the system needs to transport the L_t rotational fault to the middle of the conductor. This choice is motivated from the fact that the relaxation of a species initially distributed in one well of a symmetric double well potential is described by the mean first-passage time to the top of the barrier between the wells [26].

Approximation of the relaxation time by the mean first-passage time $\tau_{1\to j}$ is based on the not previously explicitly stated assumption that a quasi-equilibrium exists among configurations $1 \le k \le j$. If the system starts in a state near the quasi-equilibrium or can establish the equilibrium much faster than it reaches the state j, the first-passage time provides a good description. However, if two or more quasi-equilibria precede j, it may be necessary to generalize the approach. Better estimates of the relaxation times are then found by seeking a uniform approximation to the quantity that measures the relaxation of the probability distribution, the particle correlation function $N(t)$ defined in Section 4.3. We illustrate this point for the ejected conductor which reaches the state 5′ following two relaxation processes. To derive the desired description we approximate $N(t) = \sum_{i=1'}^{4'} P_i$ by a bi-exponential function $n(t)$. Requiring the approximate $n(t)$ to agree with $N(t)$ at short times [i.e. $N(0) = 1 = n(0)$ and $\dot{N}(0) = 0 = \dot{n}(0)$] results in the functional form

$$n(t) = (t_1 e^{-t/t_1} - t_2 e^{-t/t_2})/(t_1 - t_2).$$

The two relaxation times t_1 and t_2 are determined by imposing two additional conditions on the moments

$$\int_0^\infty \mathrm{d}t\, N(t) = \tau_{1'\to 5'} = \int_0^\infty \mathrm{d}t\, n(t)$$

$$\int_0^\infty \mathrm{d}t\, tN(t) = \tau^{(2)}_{1'\to 5'} = \int_0^\infty \mathrm{d}t\, tn(t).$$

$\tau_{1'\to 5'}$ and $\tau^{(2)}_{1'\to 5'}$ are evaluated according to (4.27) and (4.29). The relaxation times are then

$$t_{1,2} = \tau_{1'\to 5'}\left[\frac{1}{2} \pm \sqrt{\frac{\tau^{(2)}_{1'\to 5'}}{(\tau_{1'\to 5'})^2} - \frac{3}{4}}\right].$$

$t_1 \simeq 2.0 \cdot 10^{-6}$s is the time needed for the reprotonation, and $t_2 \simeq 1.2 \cdot 10^{-10}$s is the time needed to establish the translational quasi equilibrium among the configuration $1' - 4'$.

4.5. Heterogeneous conductors

We consider now the effects of a heterogeneity in the conductor upon the time-dependent observables $\Delta F(t)$, $T_R(t)$ and $\Delta\mu(t)$. In Figure 15a a proton is either injected into the acidic (left-hand) end or it is removed (ejected) from the basic (right-hand) end of an AB diode. In both cases the resulting proton transport is in the forward direction and the injection (ejection) probability is near unity, $I(P^\circ) = 0.9994$ (0.9950). Due to the pK differences in the conductor the equilibrium distribution P° locates more protons on the basic side than on the acidic side so that injection or ejection in the reverse direction would lead to values for $I(P^\circ)$ that are three to four orders of magnitude smaller.

As opposed to the homogeneous chain, the initial changes in the dipole moment $\Delta\mu(t)$ are small and are characterized in both the injection and the ejection case by a single plateau existing well beyond the millisecond range. At short times $10^{-10}\text{s} < t < 10^{-6}\text{s}$ the plateau value is determined by a translational quasi-equilibrium; however, the motions of the proton (D_t-fault) or hole (L_t-fault) in establishing this equilibrium are local and do not involve migration over the entire conductor. Around 10^{-6}s isolated

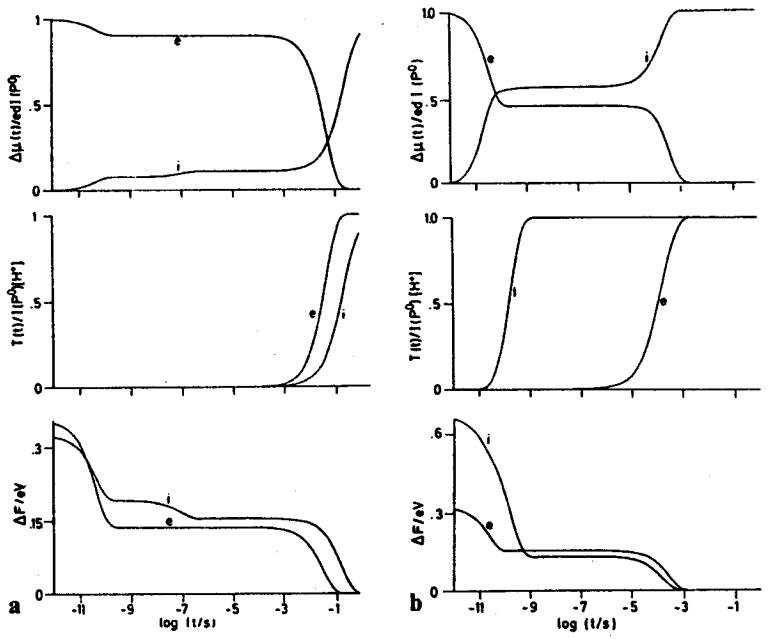

Fig. 15. Comparison of the responses of an AB-diode (a) and of a field diode (b) after the injection (i) at group 1 or ejection (e) at group 4. The calculated quantitities are defined in Fig. 14 and the text. The integrated current $T(t)$ is measured at the left for ejection (e)

internal rotations occur, but since the configurations are less probable, the accompanying changes are bearly noticeable.

Relaxation of the AB diode after injection of a proton is primarily determined by the deprotonation step at the basic end ($K_D(BH_2) \simeq 2 \cdot 10^3 s^{-1}$). The complete restoration, however, requires almost a second due to the competition between reprotonation ($K_P(BH) \simeq 10^5\ s^{-1}$) and rotation ($K(O \rightarrow L_r) \simeq 10^4 s^{-1}$) of the basic end group.

The behavior of a field diode after injection of a proton at the left side or the ejection of a proton at the right side is shown in Fig. 15b. Like the AB diode substantial transport is possible only in the forward direction in which case $I(P^\circ)$ is near unity. The Φ_ε-graphs of the integrated fluxes exhibit the same $D_t(L_t)$-L_r relaxation mechanism as for the homogeneous conductor in Section 4.4. In the case of injection, the behavior is exactly analogous as is evident from a comparison of the observable in Figs. 14a and 15b.

In the case of ejection, the response of the field diode differs considerably from that of the homogenous conductor. The internal field alters the free energy profile of Fig. 14c in that it establishes an energy decrease along configurations 1′ to 4′, an increase of the protonation barrier, and a decrease of the rotational barriers and configurations 6′ to 9′. As a result the initial relaxation of the free energy $\Delta F(t)$ is considerable as it reflects the energy decrease of 1′ to 4′. The second relaxation step in $\Delta F(t)$ for the ejected homogeneous conductor in Fig. 14a has disappeared in Fig. 15b since the protonation and the induction of the L_r fault fall in the same frequency range for the field diode. This is also shown by a comparison of the integrated proton current. Correspondingly, the dipole moment $\Delta\mu(t)$ exhibits only a single plateau which is described by the quasi-equilibrium of a linear kinetic sequence like in (4.17) involving the configurations 1′ to 4′ of Fig. 14c albeit with different free energy values. Taking into account the field-induced anisotropy in the conductor, the corresponding dipole moment change is approximated from (4.16)–(4.19) by

$$\Delta\mu(10^{-10}s < t < 10^{-5}s) = -\frac{\sum_{i=1}^{N}(i-1)\varepsilon_t^{i-1}}{\sum_{i=1}^{N}\varepsilon_t^{i-1}}\mu_t I(P^\circ)$$

where $\varepsilon_t = K(L_t \rightarrow L_t)/K(L_t \leftarrow L_t)$. One obtains the value $\Delta\mu = -0.55\ edI(P^\circ)$ which is in good agreement with the plateau value in Fig. 15b.

The mean first-passage time $\tau_{1\rightarrow N}$ provides an estimate for the time required for the initial relaxation process and $\tau_{1\rightarrow N+1} = \tau_{1\rightarrow N} + \tau_{N\rightarrow N+1}$ for the reprotonation of the ejected field diode:

$$\tau_{1\rightarrow N} = \frac{1}{K(L_t \leftarrow L_t)}\sum_{j=1}^{N-1} j\varepsilon_t^{j-N+1} \qquad \tau_{N\rightarrow N+1} = \frac{1}{K_P(X)}\sum_{j=1}^{N}\varepsilon_t^{j-N}.$$

For $N = 4$, $\tau_{1\rightarrow N} = 5.0 \cdot 10^{-11}$s and $\tau_{1\rightarrow N+1} = 1.4 \cdot 10^{-4}$s in good agreement with Fig. 15b.

5. Relaxation of a proton conductor — Group contact model

In a realistic system the interaction between a proton donating or accepting group and the conductor has a finite duration and is characterized by a finite pK difference. The finite duration of the proton transfer, the prolonged contact, and the pK changes in the injector alter the relaxation of the conductor. On the basis of the analysis developed in Section 4, we will study this relaxation and also consider more complex dynamical responses as may be realized in the "blue light effect" of bacteriorhodopsin which combines both proton injection and ejection.

In bacteriorhodopsin the injecting group could be its chromophore, a protonated Schiff base of all-trans retinal. Light absorption induces an isomerization to a 13-cis conformation. According to the model of Schulten and Tavan [27] this twisted conformer includes a 14s-cis rotation as well which renders the chromophore acidic so that the Schiff-base proton can be easily injected into a conductor in contact with the extracellular space. At room temperature, the unprotonated retinal returns within 10^{-3}s to its original protonated conformation through a series of conformational intermediates. The original protonated conformer, however, can also be obtained within 10^{-9}s through irradiation of any intermediate appearing in the cycle before 10^{-5}s. This observation, known as the "blue light effect", suggests a second or prolonged interaction of the injector group with the proton conductor, albeit with an accompanying increase in the pK value of the chromophore. A conceptual difficulty connected with the blue light effect was seen in the fact that the pumped proton appears already about 10^{-6}s after the first irradiation in the extracellular space of bacteriorhodopsin. The retrieval of this proton from the extracellular space on the time scale of a photoreaction or somewhat longer seemed impossible. We will show here, however, that the proton conductor acts as a proton buffer which releases a proton $10^{-9}-10^{-6}$s after injection but that can rapidly return the injected proton over a prolonged period and retrieve the released proton within 10^{-6}s or longer depending on the solution pH.

5.1 Technical Modifications

The total system of injector and conductor groups can be treated with few modifications by the kinetic model set up in Section 1.1. As opposed to the conductor groups, the injector is capable of accepting only a single proton. If $\Phi = (\phi_1, \phi_2, \ldots \phi_M)$ is the M-dimensional set of configurations describing the conductor and $\Gamma = (1,0)$ the two-dimensional set describing the injector's state of protonation, then the total system is described by the $2M$-dimensional set of configurations

$$\Omega_{\text{Total}} = (1 \times \phi_1, \ldots\ldots, 1 \times \phi_M, 0 \times \phi_1, \ldots\ldots, 0 \times \phi_M).$$

The time-dependent proton distribution obeys the master equation

$$\dot{P}(t) = \mathbf{K}\, P(t)$$

where the components P_i correspond to configurations in Ω_{Total}. $\mathbf{K}$ is a $2M$-dimensional matrix of rate constants describing the internal transitions, transitions between the conductor and the solution, and transitions between the conductor and the injector. We will need two different rate matrices corresponding to the situation that the injector is interacting (coupled) or not interacting (uncoupled) with the conductor. In either case, the injector is not allowed to rotate. In the uncoupled case, the rate constants are identical to those employed in the strong transfer model for both protonation states of the injector. In the coupled case, rotations of the first conductor group (in contact with the injector) are treated as if the system consisted of $N+1$ groups, e.g. its rotation give rise to the migration of an L_r or D_r fault or to the formation or destruction of an L_rD_r fault. Depending on the state of protonation of the end group (X), the protonation of the conductor by the injector (I) is described by the following transitions:

$$<1\times\phi_j|K|0\times\phi_i> = \begin{cases} K_{ij}\,(L_t^X \rightarrow L_t^I)\ \text{X unprotonated} \\ K_{ij}\,(0 \rightarrow L_t^I D_t^X)\ \text{X singly protonated.} \end{cases} \tag{5.1}$$

The rate constants for all other transitions in the coupled case are the same as in the strong injector model.

Calculation of the observables carried out in Section 4 for the strong transfer model is similarly performed here. The reference point for evaluation of the dipole moment is now the injector group so that a proton transported across the membrane gives rise to a dipole moment

$$ed = N\,\mu_r + N\,\mu_t \text{ (cf. Table 1).} \tag{5.2}$$

The equilibrium distribution used as reference for the free energy change (4.9) has two different values depending on whether the injector is coupled or not the conductor. In either case it is taken to be the asymptotic distribution of the momentary system.

5.2. Results

Figure 16 shows the response of a homogeneous conductor in contact with an injecting group for a finite period $0 \le t \le t_f = 10^{-5}$s. The transport begins at $t = 0$ when a protonated injector groups is brought into contact with the conductor in equilibrium resulting in the initial state

$$P(0) = P^\circ + \sum_{j=1}^{M} P_{0j}^\circ (e_j^1 - e_j^\circ). \tag{5.3}$$

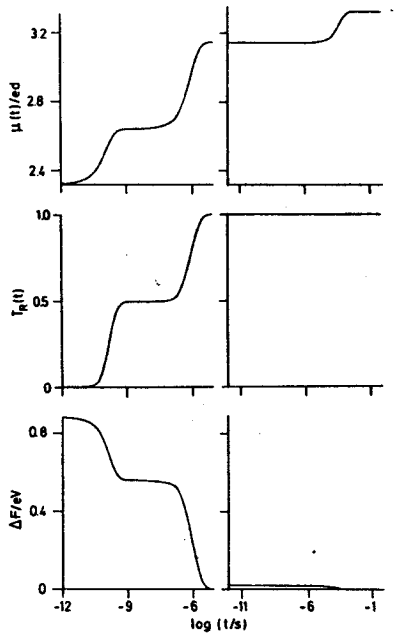

Fig. 16. Relaxation of a homogeneous conductor [pK(XH) = 10, pK(XH_2) = −2] in contact with an injector group with pK(*inj*) = −4. The solution at the right is at $pH_b = 7$. (α) at $t = 0$ the protonated injector is coupled to the conductor, (β) at $t = 10^{-5}$s the injector is removed. The calculated quantities are defined in Fig. 14 and in the text

P° is the equilibrium distribution for the uncoupled total system which does not differentiate between a protonated or unprotonated injector. P_{0j}° are the components for the j-th configuration with an unprotonated injector. e_j° (e_j^1) is the unit vector for the j-th configuration with an unprotonated (protonated) injector group. The second term shifts the weights to form the initial protonated injector state.

Since the solution at the right side is set at neutral pH = 7, the initial state I_0 obtained from (5.3) is a mixture mainly of the two neutral states α_L and α_R

$$\begin{aligned} I_0 &= 1/2\ (1|10101010|0) + 1/2\ (1|01010101|0) \\ &= 1/2\ (1|\alpha_L|0) + 1/2\ (1|\alpha_R|0). \end{aligned} \tag{5.4}$$

The state of protonation is indicated by the notation ({injector}| {conductor}| {solution}). When a proton enters the conductor in the state α_R, a D_t fault is formed. Within 10^{-9}s the proton migrates across the conductor and enters the solution which results in the translocation of 1/2 of

a proton as shown in Fig. 16. The system remains in the new state I_1 until $t = 10^{-6}$s

$$I_0 \rightarrow I_1 = 1/2\ (1|\alpha_L|0) + 1/2\ (0|\alpha_L|1).$$

The transport mechanism leading to I_1 is practically identical to that for the strong transfer discussed in Section 4.4. The plateau value in the dipole moment can be approximated from (4.11) and (5.2) using the injector as the reference point

$$\mu(I_1) = \sum_{i=1}^{N} (i\mu_t + (i-1)\mu_r) + 1/2\ (N\mu_t + N\mu_r)$$
$$= (N+2)\frac{N}{2}\mu_t + \frac{N^2}{2}\mu_r\,. \tag{5.5}$$

For $N = 4$, $\mu(I_1) = 2.64\,ed$ which is in good agreement with the exact value of (10^{-9}s $< t < 10^{-7}$s) in Fig. 16.

The time required for the system to reach the state I_1 is estimated by the first-passage time

$$\tau_{I_0 \rightarrow I_1} = \frac{N}{K_D} + \frac{N(N-1)}{2K_t} + \frac{K_D^I}{K_P^I}\left[\frac{1}{K_D} + \frac{(N-1)}{K_t}\right] + \frac{1}{K_P^I} \tag{5.6}$$

where $K_t = K(D_t \rightarrow D_t)$, $K_{P,D}^I = K(0 \leftrightarrows L_t^I D_t^X)$ are the protonation and deprotonation rate constants at the injector side, and $K_D = K_D(XH_2)$ is the deprotonation rate constant at the solution side. Upon comparing this expression to the translocation time $\tau_{1 \rightarrow N+1}$ of the strong injector model in (4.33), one sees that the last two terms are corrections for the presence of the injector. Since the injector is assumed to be acidic with respect to the conductor ($pK_t = -4$ vs. $pK_1 = 10$, $pK_2 = -2$), K_P^I is large and consequently the injector has a negligible effect on this short time phase of the transport.

The presence of the injector group makes rotation of the first conductor group easier, and this effect becomes noticeable for $t > 10^{-6}$s. Rotation of the first group initializes the migration of a D_r fault across the conductor that ends in the formation of the state from which the translocation of the remaining 1/2 proton follows as described above in the process $I_0 \rightarrow I_1$,

$$1/2\ (1|\alpha_L|0) \xrightarrow{D_r} 1/2\ (1|\alpha_R|0) \xrightarrow{D_t} 1/2\ (0|\alpha_L|1).$$

The proton transfer is now completed and the system is in the equilibrium state $I_2 = (0|\alpha_L|1)$. The rate determining step for the transport is the migration of the D_r fault

$$\tau_{I_1 \rightarrow I_2} = \frac{N(N+1)}{2K(D_r \rightarrow D_t)} = 1.14 \cdot 10^{-6}\text{s}. \tag{5.7}$$

An approximation for the dipole moment follows directly from (4.11),

$$\mu(I_2) = (N+3)\frac{N}{2}\mu_t + \frac{N(N+1)}{2}\mu_r = 3.14\ ed. \tag{5.8}$$

At $t = 10^{-5}$s, the injector is uncoupled (removed), and the conductor relaxes to a new equilibrium state I_3 that is a mixture of the two neutral states

$$I_2 \rightarrow 1/2\ (0|\alpha_R|1) + 1/2\ (0|\alpha_L|1) = I_3.$$

The state α_R and α_L are connected by a series of N rotations. Since one of the states is overpopulated at the time of the uncoupling, fifty percent of the distribution must undergo formation and migration of an L_r rotational fault to obtain I_3. The first-passage time for this final relaxation process will be in the range of the time constant for the formation of the L_r rotational fault at the end group

$$\tau_{I_2 \rightarrow I_3} = \frac{1}{K(0 \rightarrow L_r)} + \frac{(N-1)(N-2)}{2K(L_r \rightarrow L_r)} + \frac{(N-2)K(0 \leftarrow L_r)}{K(L_r \rightarrow L_r)K(0 \rightarrow L_r)}$$
$$+ \frac{1}{K(L_r \rightarrow 0)}\left[\frac{K(0 \leftarrow L_r)}{K(0 \rightarrow L_r)} + N - 1\right] = 1.1 \cdot 10^{-3}\text{s}\,. \tag{5.9}$$

The state I_3 of the uncoupled system has a dipole moment of

$$\mu(I_3) = \mu(I_2) + \frac{N}{2}\mu_r = 3.32\ ed \tag{5.10}$$

which agrees well with the calculated plateau value in Fig. 16.

At room temperature and neutral pH, the photocycle of the proton pump in bacteriorhodopsin requires milliseconds to return to its original state. It is of interest to see whether another proton could be conducted before the conductor has equilibrated. At $t = 10^{-5}$s instead of removing the injector group, a new protonated injector group is brought into contact with the conductor. Figure 17 shows the results for such a situation. Until $t = 10^{-5}$s the behavior of the system is the same as in Fig. 16 (different scaling has been employed) , i.e. the system has transported one proton and is in the state I_2 described above. Anewed protonation of the injector results in the state $I_2' = (1|\alpha_L|1)$ of considerable higher energy. As in the transition from $I_1 \rightarrow I_2$ the system awaits the migration of a D_r rotational fault ($t \simeq 10^{-6}$s) after which the translocation of a proton follows immediately

$$I_2' \rightarrow (1|\alpha_R|1) \rightarrow (0|\alpha_L|2) = I_4\,.$$

The time for the translocation is the refraction time, and it can be approximated by the first-passage time

$$\tau_{I_2' \rightarrow I_4} = \tau_{I_1 \rightarrow I_2} = 1.14 \cdot 10^{-6}\text{s}\,.$$

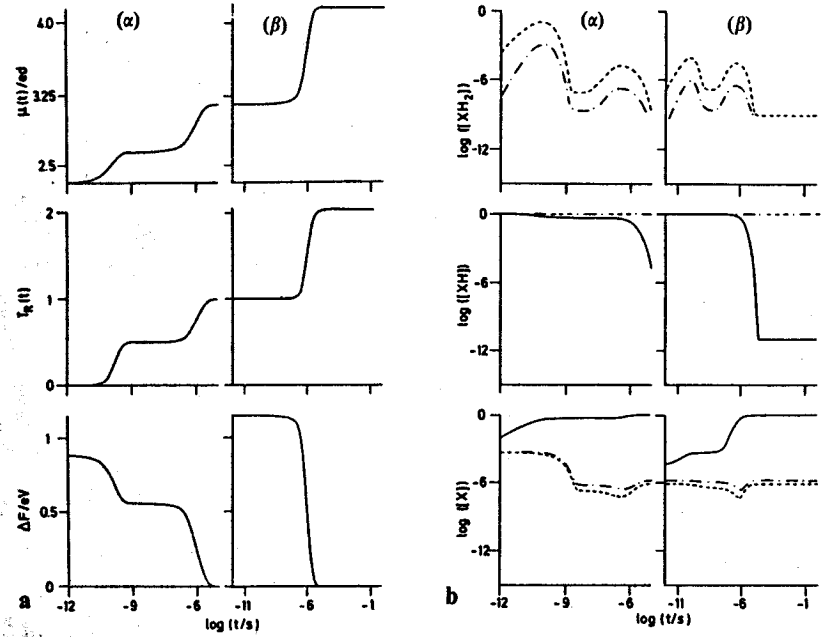

Fig. 17. Demonstration of the delay time of the homogeneous proton conductor in Fig. 16: (α) at $t = 0$ a protonated injector group is coupled to the conductor; (β) at $t = 10^{-5}$ s a new protonated injector group is brought into contact. a) The calculated quantities are defined in Fig. 14

Fig. 17. b) The protonation states of group X_I (——), X_M (– – –), and X_R (–·–·–)

A second proton could be transported after a few microseconds. During the refraction phase, the dipole moment reaches the plateau value

$$\mu(I_4) = \mu(I_2) + N\mu_t + \mu_r = 4.14\ ed.$$

The states of protonation of the injecting group X_I, a middle group X_M, and the right end group X_R of the conductor during the transport are shown in Fig. 17b. The protonation states have been evaluated according to (4.12) by means of the probabilities $[X_i]$, $[X_iH]$, and $[X_iH_2]$, $i = I, M, R$. The injector ($[X_IH_2] \equiv 0$) is initially in the state $[X_IH] = 1$. $[X_IH]$ decreases at longer times to the equilibrium value 10^{-11} at pH = 7 dictated by the injector pK,

$$\mathrm{pK(XH)} = \log \frac{[\mathrm{XH}]}{[\mathrm{X}]} + \mathrm{pH}\ . \qquad (5.11)$$

Initially the groups M and R are in an equilibrium state consisting of the two neutral configurations α_R and α_L, so that $[X_MH]/[X_M]$ and $[X_RH]/[X_R]$ satisfy (5.11) at short times. After transport of the first and second proton, the

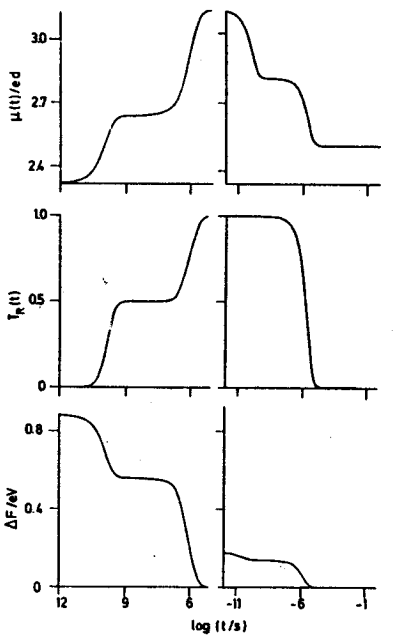

Fig. 18. "Blue light effect" on the homogeneous proton conductor in Fig. 16: (α) at $t = 0$ a protonated injector group with pK(inj) = −4 is coupled to the conductor; (β) at $t = 10^{-5}$ s a sudden change of the injector pK value occurs to pK(inj) = 10. Calculated quantities are defined in Fig. 16

effective pK-value defined according to (5.11) increase as $[X_i]$ decreases. This behavior originates from our assumption of a strong hydrogen bridge between the injector group and the left end group, i.e. the energy of formation for an L_r fault there is as high as that between the conductor groups. As a result as long as the injector is coupled, the conductor is asymptotically in the α_L configuration and, therefore, appears more basic. The probabilities $[X_MH_2]$ and $[X_RH_2]$ are seen to develop two maxima which coincide with the two phases of the proton current. This behavior is due to the fact that the proton transport involves D_t faults.

As explained above, irradiation of the intermediates appearing before 10^{-5}s in the proton pump cycle of bacteriorhodopsin results in a fast return to the original protonated retinal Schiff base. One sees from our calculations that once the injecting group has given off a proton to the conductor it is translocated to the solution within $t < 10^{-6}$ s. The question remains how, in connection with the blue light effect, the injector (the retinal Schiff base) can be reprotonated. In Fig. 18 the blue light irradiation is assumed to cause a

sudden increase in the injector's pK from −4 to 10. At the time of the pK change the system is in the state I_2. Since the injector is now basic, the first step is the abstraction of a proton from the conductor end group forming an L_t fault. The hole (L_t fault) migrates across the conductor, and the system relaxes to a new quasi-stationary distribution I_5. The new state I_5 contains those configurations involved in the transport of the L_t fault and gives rise to a decrease in the dipole moment in the range $10^{-10}\text{s} < t < 10^{-6}\text{s}$

$$\mu(I_5) = \mu(I_2) - 1/5 \frac{N(N+1)}{2} \mu_t = 2.82 \; ed.$$

Relaxation is complete after reprotonation of the conductor at the solution side around $t \simeq 10^{-6}$s. To the final state $I_6 = (1|\alpha_R|0)$ corresponds a further decrease in the dipole moment

$$\mu(I_6) = \mu(I_2) - N \mu_t = 2.50 \; ed.$$

The dipole moment does not return to the original value because the state I_6 with a basic injector group selects one of the neutral states appearing in the initial equilibrium state I_0 (5.4). The mean first-passage time for the overall reprotonation of the injector is in the microsecond range [see (4.33)]

$$\tau_{I_2 \to I_6} = \frac{N+1}{K_P} + \frac{N(N-1)}{2K(L_t \to L_t)} = 2.5 \cdot 10^{-6}\text{s}.$$

6. Response to oscillating fields and to electric field jumps

To assist in the identification of the elementary transport processes, we have calculated the response of the proton conductors and diodes to time-dependent electric fields. The calculated quantities are the observable introduced in Section 4: changes in the dipole moment and free energy, and the integrated proton current. In the case of bacteriorhodopsin, a field jump experiment using a rectangular pulse of variable duration has already been performed [28]. The effects measured there are one to two orders of magnitude larger than those predicted in this section. This discrepancy is due to the cardinal problem that besides the conduction protons many charges and dipoles within the protein and membrane contribute to the field jump response. In fact, it appears difficult to measure separately the contribution of the protons in the conductor pathway alone. We hope that the following results point out a suitable "window" to observe the elementary processes connected with proton transport in proteins.

The desired separation of proton transport from other responses may be more easily achieved in frequency space and, therefore, we have also investigated the influence of an oscillating field of variable frequency on the

observables. Being strongly damped systems, the proton conductors are not expected to exhibit strong resonances. However, in certain frequency ranges, the elementary processes of translation and protonation reveal themselves by changes in the amplitude and phase shift of the observables.

The structure of the master equation and the rate constants for time-dependent fields follows straightforwardly from Section 2. In the case of the oscillating field, the time dependence of the external electric field is sinusoidal with a frequency ν

$$V_{ext}(t) = V^{\circ}_{ext} \sin 2\pi\nu t, \tag{6.1}$$

and in the case of the electric field jump it is a step function with a pulse duration τ

$$V_{ext}(t) = \begin{cases} V^{\circ}_{ext} & 0 < t < \tau \\ 0 & t > \tau. \end{cases} \tag{6.2}$$

The matrix **K** of rate constants in (1.1) is now time dependent, and the master equation

$$\dot{P}(t) = \mathbf{K}(t)\, P(t) \quad \text{with} \quad P(0) = P^{\circ} \tag{6.3}$$

is solved using the fifth-order Gear algorithm for stiff systems [19]. The system is assumed to be initially in its equilibrium state P°.

The dipole moment $\mu(t)$, the free energy $\Delta F(t)$, the proton current at both sides of the conductor, $J_R(t)$ and $J_L(t)$, and the integrated currents $T_R(t)$ and $T_L(t)$ have been calculated as in Section 4. In the case of the oscillating field, calculation of the observables begin after the initial oscillations have reached a steady period. The transient behavior disappears usually after 10−20 periods. The amplitude is taken as the difference between the maximum and minimum in a period. The phase is defined to be the shift of the dipole moment maximum to the maximum of the oscillating field. For the field jump calculations, the nontrivial test for stability

$$\lim_{t \to \infty} [T_R(t) - T_L(t)] = 0$$

is made after the system has relaxed at $t = 1$ sec. Convergence tests were used to determine the tolerance parameter $\text{tol} = 0.0001$ and the step length parameters $h_J = 10^{-14}$ (field jump) and $h_0 = 10^{-4}/\nu$ (oscillating field) required in the Gear algorithm.

Figure 19 depicts the response of a homogeneous conductor to an oscillating field of variable frequency ν. Both ends of the conductor are in contact with an aqueous solution at pH = 7. The phase shift of $\Delta\mu$ at the bottom of Fig. 19 shows that the dipole moment is in phase with the oscillating field at frequencies $10^7\,\text{Hz} < \nu < 10^9\,\text{Hz}$. Corresponding to this minimum in the phase shift, the amplitude $\log(\Delta\mu/ed)$ exhibits a plateau

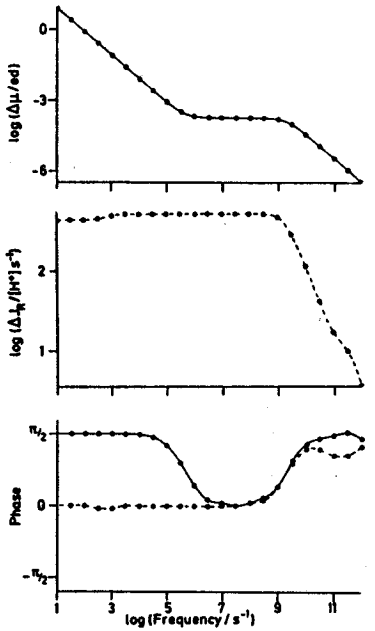

Fig. 19. Frequency dependence of the dipole moment and proton current of a homogeneous conductor at pH = 7 [$N = 4$, pK(XH) = 10, pK(XH_2) = −2] in an alternating electric field with amplitude $V^{\circ}_{ext} = 25$ mV: (——) amplitude $|\Delta\mu(t)|$ and phase of the dipole moment; (– – – –) amplitude $|\Delta J_R(t)|$ and phase of the proton current

value. The time-dependent distribution $P(t)$ reveals that in this frequency range configurations α_i connected by translation of an L_i fault across the conductor form a distribution that is quasi-adiabatic

$$\alpha_1 \underset{k_{-1}(V_{ext})}{\overset{k_1(V_{ext})}{\rightleftharpoons}} \alpha_2 \underset{k_{-2}(V_{ext})}{\overset{k_2(V_{ext})}{\rightleftharpoons}} \alpha_3 \cdots\cdots \underset{k_{-N+1}(V_{ext})}{\overset{k_{N-1}(V_{ext})}{\rightleftharpoons}} \alpha_N,\ \alpha_i \in \Omega(L_i). \tag{6.4}$$

Each configuration in $\Omega(L_i)$ has exactly one L_i fault, and $k_i(V_{ext})$ is the time-dependent rate constant for the migration of the L_i fault obtained from (2.3), i.e. $k_i(V_{ext}) = K[L_i \to L_i](t)$.

The dipole moment resulting from oscillations within this quasi-adiabatic distribution $\hat{P}_\alpha$ can be approximated from (4.10)

$$\mu(t) = \sum_{\alpha\in\Omega} \mu(\alpha)\hat{P}_\alpha(t) + \sum_{\beta\notin\Omega} \mu(\beta)\, P^{\circ}_\beta + ed\, T_R(t). \tag{6.5}$$

P° is the equilibrium distribution. The configurations in Ω are identical to those in the short-time quasi-stationary distribution of the ejected conductor

in Section 4.4. Allowing for time-dependent rate constants in (4.18) and (4.19), a similar derivation for $\hat{P}_\alpha(t)$ is possible,

$$\hat{P}_i(t) = N_\Omega \prod_{j=1}^{i-1} \frac{k_j(V_{ext})}{k_{-j}(V_{ext})}. \tag{6.6}$$

The normalization factor N_Ω follows from the condition

$$\sum_{\alpha\in\Omega} P_\alpha(t) = \sum_{\alpha\in\Omega} P^{\circ}_\alpha = S. \tag{6.7}$$

The amplitude $|\Delta\mu|$, defined as the maximum minus the minimum value of $\mu(t)$ over a period, is within this approximation

$$|\Delta\mu(10^7\text{Hz} < \nu < 10^9\text{ Hz})| \simeq |\Delta\mu[\Omega(L_i)]| = S\mu_i[\delta(\varepsilon_i) - \delta(\varepsilon_i^{-1})] \tag{6.8}$$

where

$$\delta(\varepsilon_i) = \frac{\sum_{i=1}^{N} (i-1)\varepsilon_i^{i-1}}{\sum_{i=1}^{N} \varepsilon_i^{i-1}}.$$

ε_i is the correction to the rate constants from the oscillating field with amplitude V°_{ext}

$$\varepsilon_i = \exp(\mu_i f\beta V^{\circ}_{ext}/d) \qquad (\beta = 1/kT). \tag{6.9}$$

With the equilibrium distribution P° known from the stationary state calculations, one obtains $|\Delta\mu(\Omega)| = 1.75 \cdot 10^{-4} ed$ which compares well with the exact value of $\Delta\mu = 1.748 \cdot 10^{-4} ed$ at 10^8 Hz.

At frequencies higher than 10^9 Hz or smaller than 10^7 Hz, the phase of the dipole moment goes to the value $\pi/2$. This result can be understood on the basis of a simple model of a two component reaction

$$A \underset{k'}{\overset{k}{\rightleftharpoons}} B$$

with the time-dependent rate constants

$$k = k_0 \exp(\alpha \sin \omega t)$$

$$k' = k_0 \exp(-\alpha \sin \omega t)$$

where $\alpha = \beta\mu V^{\circ}_{ext}/2d$ and k_0 is time independent. For small fields the rate equations

$$\dot{P}_A = -k\, P_A + k'\, P_B$$

$$\dot{P}_B = -k'\, P_B + k\, P_A$$

can be reduced to the simple differential equation

$$\dot{P}_A + 2k_0 P_A = k_0 (1 - \alpha \sin \omega t).$$

P_B is obtained from the condition $P_A + P_B = 1$. $P_A(t)$ has the solution

$$P_A(t) = c e^{-2k_0 t} + 1/2 - \Delta \sin (\omega t - \Theta)$$

where c is a constant. The phase shift and the amplitude of the sinusoidal term are

$$\Theta = \arccos [2k_0/\sqrt{(2k_0)^2 + \omega^2}]$$

$$\Delta = k_0 \alpha/\sqrt{(2k_0)^2 + \omega^2}\,.$$

The initial transient behavior decays away with a time constant $(2k_0)^{-1}$ after which the system undergoes oscillations that are shifted by a phase Θ from the applied electric field of frequency ω. Two limiting cases are of interest: i) if $\omega \gg k_0$, then $\Theta = \pi/2$ and $\Delta = 0$; ii) if $\omega \ll k_0$, then $\Theta = 0$ and $\Delta = \alpha/2$ (the system follows the oscillating field quasi-adiabatically). These two simple cases allow us to qualitatively explain Fig. 19.

At high frequencies, $\omega \gg k_0 = K(L_t \rightarrow L_t)$, no concerted transitions between the configurations in (6.4) will take place. The phase of the distribution and, therefore, that of the dipole moment will be shifted by $\pi/2$. The rise in the phase of the dipole moment at frequencies below 10^7 Hz is due to the onset of processes slower than the translations, e.g. protonation occurs with a rate constant of $2 \cdot 10^6 s^{-1}$.

Below 10^2 Hz, a quasi-adiabatic proton current flows in phase with the oscillating field across the conductor. The amplitude of the current ΔJ_R at 10 Hz is exactly the stationary current $J_R = 2.31 \cdot 10^2$ protons s^{-1} obtained when a constant field of strength $V_{ext} = 25$ mV is applied. The dipole moment is here principally determined by the integrated current $T_R(t)$ [see (6.5)] and therefore follows the field by a phase of $\pi/2$.

Figure 20 presents the behavior of the system in Fig. 19 submitted, however, to an electric field jump of duration $\tau = 10^{-4}$s and strength $V_{ext} = 10$ mV. At short times 10^{-9}s $< t < 10^{-7}$s after the beginning of the jump, the field induces a quasi-equilibrium analogous to the quasi-adiabatic state Ω existing in the 10^7 Hz–10^9 Hz region in Fig. 19. The corresponding small plateau value of $\Delta\mu(t)$ estimated by the expression

$$\Delta\mu[\Omega(L_t)] = \mu_t S [\delta(\varepsilon_t) - \delta(0)] = 3.53 \cdot 10^{-5}\, ed$$

is in good agreement with the numerical value. At longer times the field induces a proton current. The major part of the current is irreversible since the solution is assumed to be buffered at pH = 7. A minor part of the current as well as of the dipole moment reverses after switch off.

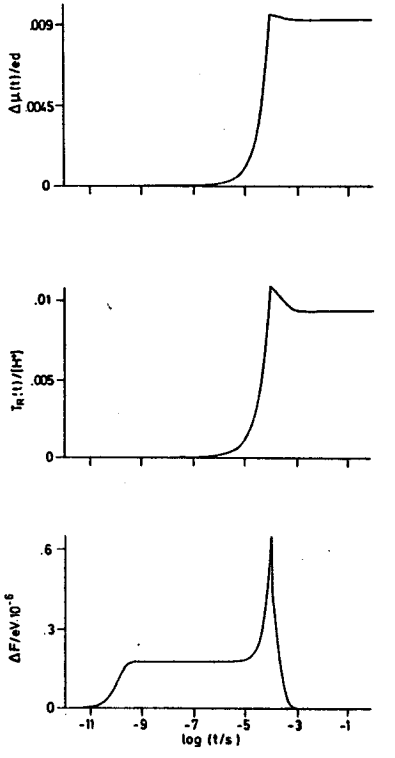

Fig. 20. Response of the homogeneous conductor in Fig. 19 to a field jump experiment at pH = 7; duration of the jump is 10^{-4} s with amplitude $V^{\circ}_{ext} = 10$ mV. The observable calculated are the dipole moment $\Delta\mu(t) = \mu(t) - \mu(0)$, the integrated proton current $\int J_R\, dt$, and the change in free energy $\Delta F(t)$

We have also examined the influence of pH on the above investigations, and in Fig. 21 we present analogous calculations at pH = 10. The quasi-adiabatic (stationary) distribution (6.4) again determines the dipole moment in the region 10^7 Hz $< \nu < 10^9$ Hz (10^{-10}s $< t < 10^{-7}$s). The plateau value of $\Delta\mu$ corresponding to this translational process is now larger in the field jump case. The pH dependence of the amplitude $\Delta\mu(t)$ follows directly from the pH dependence of the equilibrium distribution P°. At pH = 10 a second plateau develops in the range 10^3 Hz $< \nu < 10^5$ Hz (10^{-6}s $< t < 10^{-5}$s). It involves a quasi-adiabatic (quasi-stationary) distribution of configurations that are coupled through translations of an L_t fault and protonation

$$\alpha_0 \underset{K^*_P}{\overset{K^*_D}{\rightleftharpoons}} \alpha_1 \underset{K(L_t \leftarrow L_t)}{\overset{K(L_t \rightarrow L_t)}{\rightleftharpoons}} \alpha_2 \underset{K(L_t \leftarrow L_t)}{\overset{K(L_t \rightarrow L_t)}{\rightleftharpoons}} \cdots\cdots \alpha_N \underset{K^*_D}{\overset{K^*_P}{\rightleftharpoons}} \alpha_{N+1} \qquad (6.10)$$

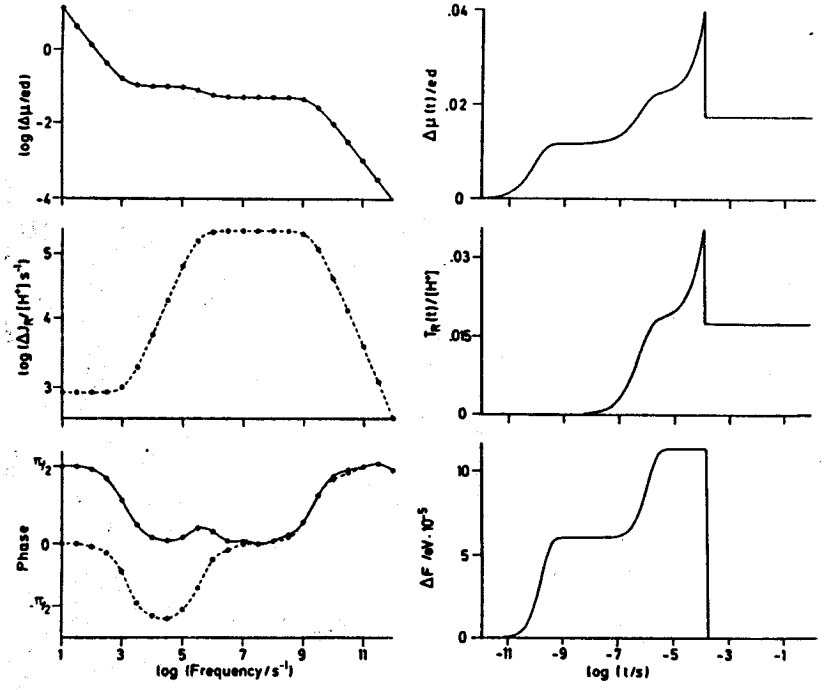

Fig. 21. Response of the homogeneous conductor to (a) an alternating electric field and to (b) a field jump with conditions and observables as in Figs. 19 and 20 but with pH = 10

The amplitude of the dipole moment associated with this quasiadiabatic translocation oscillation can be estimated with the aid of Eqs. (6.5)–(6.8)

$$|\Delta\mu(10^3\,\text{Hz} < \nu < 10^5\,\text{Hz})| \simeq \mu_t\Big(\sum_{i=0}^{N+1} P_i^\circ\Big)\,[\delta(\varepsilon_t) - \delta(\varepsilon_t^{-1})] \qquad (6.11)$$

with

$$\delta(\varepsilon_t) = \frac{\sum_{i=1}^{N} (i-1)\,\varepsilon_t^{i-1} + (N-1)\,\varepsilon_t^{N-1}\,K_P^\flat/K_D^\flat}{\sum_{i=1}^{N} \varepsilon_t^{i-1} + \varepsilon_t^{N-1}\,K_P^\flat/K_D^\flat + K_P^a/K_D^a}\,.$$

With the equilibrium distribution known from the stationary-state calculations, one obtains from (6.11) $|\Delta\mu(10^3\,\text{Hz} < \nu < 10^5\,\text{Hz})| \simeq 1.1 \cdot 10^{-1}\,ed$ for pH = 10 and $N = 4$. In the case of the translocation oscillation (6.10), the proton current J_R is maximal when the change of the field is greatest, i.e. when the oscillating field goes through zero. Hence, J_R will be in advance of the field

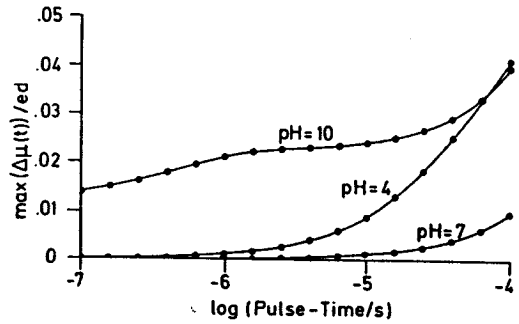

Fig. 22. Maximum dipole moment change of a homogeneous conductor $N = 4$, pK(XH) = 10, pk(XH_2) = −2 in an electric field jump experiment as a function of the pulse duration at pH = 4,7, and 10

by a phase shift of $-\pi/2$, and the integrated current T_R and the dipole moment will be in phase with the field as shown in Fig. 21 c.

In order to relate more closely our calculations to a field jump measurement, we have plotted in Fig. 22 the maximal change in the dipole moment at various pH's as a function of the pulse duration τ. The curves reflect the profiles given in Figs. 20 and 21. The amplitude $V_{ext}^\circ = 10\,\text{mV}$ is a typical value employed in the experiments on the protein bacteriorhodopsin [28]. The calculated change in $\Delta\mu$ of $2 \cdot 10^{-2}\,ed$ lies in the range of 1 Debye and is only 1% of the observed value. This large discrepancy cannot be explained by our choice of V_{ext}° or N. As stated before, the experiments measure the motions of all charges and dipoles in the protein, and at the moment one cannot separate out the contributions from the proton conductors.

As the field jump and oscillating field experiments provide rather similar information, only the latter will be discussed for the proton diodes. Figure 23 is a comparison of results for the AB and field diodes described in Section 3.4. In the case of the AB diode, the presence of a quasi-adiabatic distribution in the region $10^5\,\text{Hz} < \nu < 10^{10}\,\text{Hz}$ is evident by the constant value of the dipole moment amplitude. The time-dependent distribution reveals that isolated proton translations, separate for the acidic and basic sections of the diode, are primarily taking place. Other motions are relatively improbable until one comes into the frequency range for (de-)protonation and formation of an L_r rotational fault below 10^4 Hz. The system establishes a new quasiadiabatic distribution involving (de-)protonation at the basic end, but no net transport of a proton occurs. A proton is taken up or given off in phase with the field which explains the $-\pi/2$ phase shift in J_R in Fig. 23.

At frequencies below 10^2 Hz, the AB diode begins to function as a rectifier in that more protons are periodically transported in the forward direction than in the reverse direction. At high frequencies, the proton current J_R is in

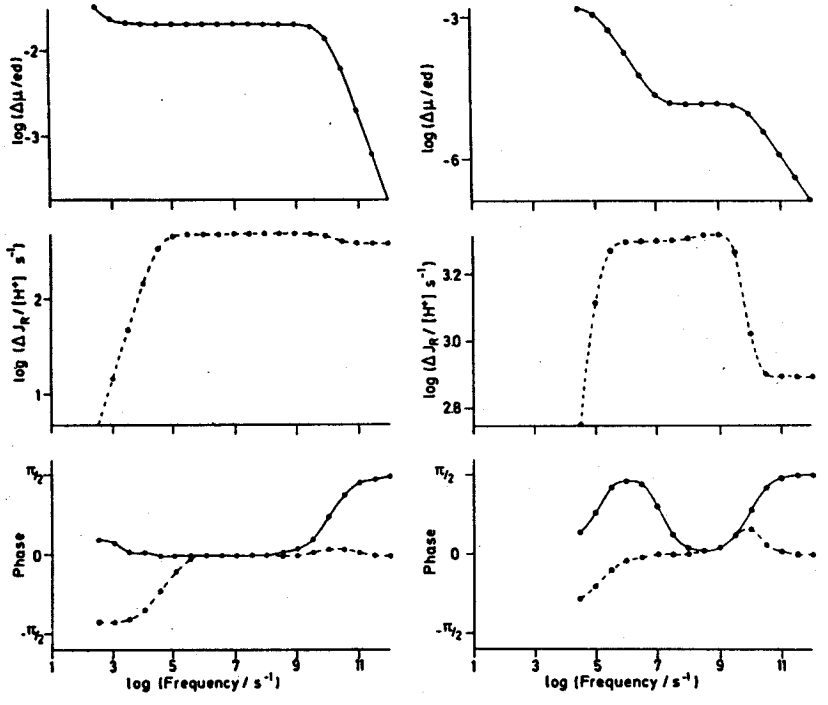

Fig. 23. Comparison of the frequency dependence of the dipole moment and proton current of the acid-base diode (a) and the field diode (b) in an alternating electric field with amplitude $V_{ext}^{\circ} = 25\,\text{mV}$. The observables are defined as for Fig. 19

phase with the field due to the field dependence in the (de-)protonation rate constants.

Similar low and high frequency behavior is exhibited by the field diode. The translational and translocational quasi-adiabatic distributions described in the discussion of the homogeneous conductor exist around 10^9 Hz and 10^4 Hz, respectively. The translocation oscillation (6.10) is now more clearly manifested by the proton current.

7. Summary

In this paper we have studied in quantitative detail a model for the proton transport through hydrogen-bridge networks in order to further develop the necessary network thermodynamic description as well as to guide the experimental study of biological proton conductors. We have formulated in Section 2 the problem of proton transport in terms of a master equation

connecting all the possible distributions of protons in the conductor. We provide theoretical algorithms for the solution of stationary (Section 3) and nonstationary (Sections 4–6) situations including time-varying external electrical fields. Extensive treatment was only possible due to the development of an algorithm for presenting out of the large space of proton distributions the kinetic pathways involved in the proton transport. The algorithm provided us with maps of all essential kinetic fluxes contributing to the transport, for example as in Fig. 9b. This knowledge underlied all our discussions and interpretations above. We decided, however, to limit the presentation to the simplest examples which allow analytical approximations for the observables connected with the transport.

The results presented concern mainly the question which observables can best reveal dynamical and structural details of proton conductors. To this end we have first considered the (titration) measurement in Figs. 3 and 7 of the stationary proton current induced by a constant electrical voltage as a function of the external pH. Such titration curves reveal the pK-values of the conducting groups. We have also analyzed in detail the elementary proton motions involved in the transport and have developed analytical expressions for the proton current and proton resistance. These approximations were obtained by reducing the kinetic pathways to a small number of effective rate limiting steps and by invoking the approach of linear irreversible thermodynamics (see Fig. 8).

Time-dependent observation are more revealing about the dynamical processes, and we have considered, therefore, proton transport after injection/ejection and in time-varying fields. For this purpose we have studied the behavior of key quantities which admit experimental investigation: free energy decrement, proton release, charge displacement, and protonation state of conducting groups (Figs. 14–16). After proton injection or ejection these observables exhibit several relaxation steps connecting quasi-stationary states of the conductor. These states are also found to play a central role under time-varying field conditions (oscillating fields and field jumps). By means of the first-passage time approximation the relaxation times can be expressed analytically in terms of the kinetic rate constants for the elementary processes [for example see Eq. (4.33)]. The quasi-stationary values of the observables are found to reveal structural details about the conductors. Under the application of oscillating fields the quasi-adiabatic distributions and relaxation processes show up as transitions in the amplitude and phase of the observables in certain frequency ranges (Figs. 19 and 23). Field jump experiments provide equivalent information (Figs. 20–22).

We have also studied possible functional characteristics of proton conductors. An important result is that conductors composed of heterogeneous (acidic and basic) groups or homogeneous groups subjected to an internal electric field can achieve diodic character, i.e. a non-linear chemiosmotic potential current characteristic as seen in Figs. 9–13. As biological

proton transport is mostly unidirectional such diodic character constitutes a very important feature.

By allowing the interaction between the conductor and injecting or ejecting group to be time and pK dependent, we have investigated in Fig. 17 the refractory phase of the conductors: after an initial proton current pulse, the conductor is left in a polarized state; repolarization involves hydrogen-bond breaking and group rotation. We have found that after an initial relaxation step a second proton can be transported before complete repolarization or recovery is achieved. We also established that a conductor can act as a proton buffer (Fig. 18): although an injected proton will be conducted and released within 10^{-6} s, a sudden change in the injector's pK even after 10^{-6} s can force the almost immediate return of a proton to the injector and the conductor to retrieve a proton from the solution at a later time t. The time t depends of the solution pH. This chain of processes is assumed to contribute to the "blue light effect" of bacteriorhodopsin.

Finally, we would like to comment on two possible critiques of the model regarded here: 1) the rate constants employed for the elementary transport processes may not be realistic; 2) certain elementary processes involving the concerted motion of several protons are not included in the description. To the first point, many of our results can be extended without further calculations to account for different rate constants. For example, a relaxation step governed by a rotational rate constant would be shifted in time or frequency space according to the suggested change. In the case of concerted transitions one could easily identify in the pathways discussed above where such transitions provide a short cut and determine if their existence would alter significantly the behavior of the conductors. For example, a concerted proton translation according to Zundel *et al.* [15] would directly connect states 1 and 4 as well as 1′ and 4′ in Fig. 14b, c and, thereby, decrease the initial relaxation times reflected by the observables in Fig. 14a to below 10^{-10} s.

Our aim has been to provide a general framework in which the behavior of complex biological proton transport can be discussed, and we hope that our results will be a stepping stone toward the illucidation of the structural basis of the transport processes connected with the chemiosmotic principle of bioenergetics.

Acknowledgement

Our investigations have greatly benefited from helpful discussions with Prof. D. Oesterhelt. The authors would also like to thank Prof. S. F. Fischer and Prof. A. Weller for their support of this work. This project has been financially supported by the Deutsche Forschungsgemeinschaft under the grant Fi 303/1-1 and the Sonderforschungsbereich "Primärprozesse bei der bakteriellen Photosynthese" (SFB 143).

References

1. P. Mitchell, Science **206** (1979) 1148.
2. H. Okamoto, N. Sone, H. Hirata, M. Yoshida and Y. Kagawa, J. Biol. Chem. **252** (1977) 6125; N. Nelson *et al.*, Proc. Natl. Acad. Sci. USA **74** (1977) 2375.
3. D. Oesterhelt, Angew. Chem. Int. Ed. Engl. **15** (1976) 17; The most recent review is W. Stoeckenius and R. Bogomolini, Annu. Rev. Biochem. (1981) in press.
4. Yu. A. Ochinnikov, N. Abdulaev, N. Feigina, A. Kiselev and N. Lobanov, FEBS Lett. **100** (1979) 219.
5. M. Eigen and L. DeMayer, Proc. R. Soc. (London), **A247** (1958) 505; M. Eigen, Angew. Chem. Int. Ed. Engl. **3** (1964) 1.
6. L. Onsager, in *Neurosciences*, ed. F. O. Schmitt (Rockerfeller University Press, New York, (1967) 75 – 79.
7. J. F. Nagle and H. J. Morowitz, Proc. Natl. Acad. Sci. USA **75** (1978) 298; J. F. Nagle, M. Mille and H. Morowitz, J. Chem. Phys. **72** (1980) 3959.
8. A. Dunker and D. Marvin, J. Theor. Biol. **72** (1978) 9.
9. S. F. Fischer, G. L. Hofacker and J. R. Sabin, Phys. Kondens. Mat. **8** (1969) 268; J. R. Sabin, S. F. Fischer and G. L. Hofacker, Int. J. Quant. Chem. **3** (1969) 257.
10. J. K. Fung, K. Godzik and G. L. Hofacker, Ber. Bunsenges. Phys. Chem. **77** (1973) 980.
11. P. Läuger, Biochem, Biophys. Acta **311** (1973) 423.
12. E. W. Knapp, K. Schulten and Z. Schulten, Chem. Phys. **46** (1980) 215.
13. D. Edmonds, Chem. Phys. Lett. **65** (1979) 429.
14. J. Schnakenberg, Rev. Mod. Phys. **48** (1976) 571.
15. H. Merz and G. Zundel, Biochem. Biophys. Res. Commun. **101** (1981) 540.
16. J. Del Bene, J. Chem. Phys. **72** (1980) 3423.
17. G. Wagner, A. DeMarco and K. Wüthrich, Biophys. Struct. Mech. **2** (1976) 139.
18. I. Munro, I. Pecht and L. Stryer, Proc. Natl. Acad. Sci. USA. **76** (1979) 56.
19. *IMSL Reference Manual* (Internal Mathematical and Statistical Libraries, Inc. Houston, (1980, 8 ed.) vol. 1.
20. R. P. Sheridan, R. M. Levy and F. R. Salemme, Proc. Natl. Acad. Sci. USA, **79** (1982) 4545.
21. L. A. Drachev, A. D. Kaulen and V. P. Skulachev, FEBS Lett. **87** (1978) 161.
22. D. R. Ort and W. W. Parson, Biophys. J. **25** (1979) 355.
23. H. Garty, S. R. Caplan and D. Cahen, Biophys. J. **37** (1982) 405.
24. B. Hess and D. Kuschmitz, FEBS Lett. **100** (1979) 334.
25. G. Weiss, *First-Passage Time Problems for One-Dimensional Random Walks*, preprint, 1980.
26. K. Schulten, Z. Schulten and A. Szabo, J. Chem. Phys. **74** (1981) 4426.
27. K. Schulten and P. Tavan, Nature **272** (1978) 85.
28. K. Tsuji and E. Neumann, FEBS Lett. **128** (1981) 265.
29. Eq. (2.6) was derived in Ref. 12 with $\Delta pK = 0$ and assumed diffusion-controlled reactions of the ions as well as the water molecules with the conductor ends. This assumption may be unreasonable for the process involving water as a reactant. One may rather assume that the appearance of a water molecule as a proton donor or acceptor is very rapid compared to the proton transfer step and replace (2.6) by

$$K_P = \frac{k_d}{2}\, 10^{-pH} + k_i' \frac{1}{1 + k_{-i}\tau}$$

$$K_D = k_i \frac{1}{1 + k_{-i}\tau} + \frac{k_d}{2}\, 10^{pH-14}.$$

$k_{\pm i}$ ($k'_{\pm i}$) are the pK-dependent rate constants for the transfer of a proton between the end group BH(B) and water. τ is a structural relaxation time for water and k_d is the bimolecular diffusion-controlled reaction rate constant for the ions.